Journal of Fluids and Structures 49 (2014) 360–385

Contents lists available at ScienceDirect

Journal of Fluids and Structures

journal homepage: www.elsevier.com/locate/jfs

Dynamics of a pipe conveying fluid flexibly restrained at the ends

M. Kheiri, M.P. Païdoussis *, G. Costa Del Pozo [1], M. Amabili

Department of Mechanical Engineering, McGill University, 817 Sherbrooke Street West, Montreal, QC, Canada H3A 0C3

ARTICLE INFO

Article history:
Received 15 April 2013
Accepted 6 November 2013
Available online 21 July 2014

Keywords:
Pipe conveying fluid
Flexible end-conditions
Argand diagram
Open system

ABSTRACT

The subject of this paper is the study of dynamics and stability of a pipe flexibly supported at its ends and conveying fluid. First, the equation of motion of the system is derived via the extended form of Hamilton's principle for open systems. In the derivation, the effect of flexible supports, modelled as linear translational and rotational springs, is appropriately considered in the equation of motion rather than in the boundary conditions. The resulting equation of motion is then discretized via the Galerkin method in which the eigenfunctions of a free-free Euler–Bernoulli beam are utilized. Thus, a *general* set of second-order ordinary differential equations emerges, in which, by setting the stiffness of the end-springs suitably, one can readily investigate the dynamics of various systems with either classical or non-classical boundary conditions. Several numerical analyses are initially performed, in which the eigenvalues of a simplified system (a beam) with flexible end-supports are obtained and then compared with numerical results, so as to verify the equation of motion, in its simplified form. Then, the dynamics of a pinned-free pipe conveying fluid is systematically investigated, in which it is found that a pinned-free pipe conveying fluid is generally *neutrally* stable until it becomes unstable via a Hopf bifurcation leading to flutter. The next part of the paper is devoted to studying the dynamics of a pinned-free pipe additionally constrained at the pinned end by a rotational spring. A wide range of dynamical behaviour is seen as the mass ratio of the system (mass of the fluid to the fluid+pipe mass) varies. It is surprising to see that for a range of rotational spring stiffness, an increase in the stiffness makes the pipe *less* stable. Finally, a pipe conveying fluid supported only by a translational and a rotational spring at the upstream end is considered. For this system, the critical flow velocity is determined for various values of spring constants, and several Argand diagrams along with modal shapes of the unstable modes are presented. The dynamics of this system is found to be very complex and often unpredictable (unexpected).

1. Introduction

Today, there is no doubt that the pipe conveying fluid has established itself as a *generic* dynamical paradigm, displaying a *kaleidoscope* of interesting dynamical behaviour. In fact, this paradigm should be regarded as a new model problem for the

* Corresponding author. Tel.: +1 514 398 6294; fax: +1 514 398 7365.
E-mail address: michael.paidoussis@mcgill.ca (M.P. Païdoussis).
[1] Present address: AMEC, Oakville, ON, Canada L6H 6X7.

http://dx.doi.org/10.1016/j.jfluidstructs.2013.11.023
0889-9746/

study of stability of structures, along with other classical model problems, such as the column subjected to a compressive load and the rotating shaft. Some reasons as to why this is so are that: (i) this is a physically simple system which can easily be modelled mathematically; (ii) it is a system for which both theoretical and experimental investigations can fairly easily be carried out; (iii) it is the simplest possible fluid–structure interaction system which can reasonably easily be adapted to display a wide variety of the dynamics of more complex engineering systems.

Although some work pertinent to the topic of pipes conveying fluid was made in the late 1800s, the first *serious* study, as discussed by Païdoussis and Li (1993), of the dynamics of pipes conveying fluid was done by Bourrières (1939), who correctly obtained the equations of motion, did some remarkable analysis and drew accurate conclusions regarding stability, especially for the cantilevered system. Later, several researchers, who were unaware of Bourrières' work, restarted the study of the dynamics of pipes conveying fluid; among them, the work of Ashley and Haviland (1950) on the vibrations observed in the Trans-Arabian Pipeline and the studies made by Feodos'ev (1951) and Housner (1952) on the dynamics of pipes supported at both ends should be mentioned.

It is now well-known that a pipe with both ends supported, a *gyroscopic conservative* system in Ziegler's (1968) nomenclature, loses stability via a pitchfork bifurcation leading to divergence, whereas a cantilevered pipe conveying fluid, an inherently nonconservative system (i.e. independently of dissipation), may lose stability at sufficiently high flow velocity via a Hopf bifurcation leading to flutter. This latter system is capable of displaying a seemingly never-ending variety of interesting and often surprising behaviour, compared to the supported-ends systems. Indeed, from now on, our main attention will be focused on the historical development in theoretical and experimental studies pertaining to the cantilevered system, albeit in an abbreviated and selective manner. For comprehensive reviews of the research undertaken on the dynamics of pipes conveying fluid, the interested reader is referred to Païdoussis and Li (1993), Païdoussis (1998); Païdoussis (2010) and Ibrahim (2010, 2011).

After Bourrières, the next remarkable study was conducted by Benjamin (1961a,b), on the dynamics of articulated cantilevers conveying fluid. He established the appropriate form of the Lagrangian equations to derive the equations of motion for *open* systems and also used the corresponding form of Hamilton's principle to derive the partial differential equation of motion of a continuously flexible elastic tube. This equation was found to agree exactly with one obtained by Niordson (1953).

Benjamin's work was further extended by Gregory and Païdoussis (1966a,b) to cases of continuously flexible pipes. They used a Newtonian approach to re-derive the equations of motion and used an exact method, followed by quasi-analytical and numerical solutions as well as Galerkin's method, to determine the conditions of stability of a system constrained to move in a horizontal plane. They also did several experiments, both with elastomer and metal pipes, to check various aspects of the theory. Later, Païdoussis (1970) studied the dynamics and stability of *hanging* and also *standing* cantilevered pipes, both theoretically and experimentally. It was found that the hanging system behaves essentially similar to the horizontal one, only with higher critical flow velocities, while the standing system was found to be more interesting. The dynamics and stability of pipes conveying fluid were further investigated by Païdoussis and Issid (1974), particularly for cases where the flow velocity had a small harmonic component superposed.

The extended version of Hamilton's principle for systems whose constituent particles change with time (open systems), initially formulated by Benjamin (1961a), in a more general form, which can also be used for open systems of changing mass, was considered by McIver (1973). This statement of Hamilton's principle for open systems was utilized in several studies; e.g. by Laithier and Païdoussis (1981) and Pramila et al. (1991) for Timoshenko pipes. In a very recent paper by Casetta and Pesce (2013), a more consistent and complete form of Hamilton's principle for open systems, or *non-material volumes* as called by the authors, has been derived. As will be discussed further in Section 3.1, McIver's (1973) statement of Hamilton's principle may still be used for derivations, provided that some additional assumptions, consistent with the system, are made.

As of 1970, more complex fluid-conveying pipe systems have been studied, *modified* by the addition of spring supports or end masses, for instance. In some cases the modified systems may become very rich dynamically, sometimes showing surprising behaviour. For example, Chen (1971) considered the case of a cantilevered pipe additionally supported at the free end by a translational spring. It was found that, if the spring is weak, the system loses stability by flutter, as the system mimics a cantilevered system, while it loses stability by divergence if the spring is stiff, similar to a clamped–pinned system. Moreover, the post-critical dynamical behaviour of the system was found to be quite complex, with the possibility of regaining stability and losing it again after. Several studies were conducted to examine the case of a spring support elsewhere along a cantilevered pipe, other than at the free end, theoretically and/or experimentally; see, for example, Edelstein and Chen (1985), Jendrzejczyk and Chen (1985) and Sugiyama et al. (1985). Moreover, the case where the downstream end of the cantilevered pipe is supported by both a translational and a rotational spring and the flow is either steady or pulsatile was considered by Noah and Hopkins (1980).

While many studies have been undertaken so far on the dynamics of modified systems in which the modifications are introduced at the downstream end, there are very few studies, to the best of authors' knowledge, in which such modifications have been made to the upstream end. Stability of a pinned-free pipe conveying fluid with a rotational spring at the pinned (upstream) end was studied by Guran and Plaut (1994a). In that paper, the stiffness of the rotational spring was assumed to have a constant part and a flow-dependent part increasing with flow velocity. It was found that there is a range of spring stiffness in which an increase of stiffness causes the critical flow velocity to decrease. It was also found that a minimum critical flow velocity exists, which is independent of the spring stiffness and is only dependent on the mass ratio of the pipe–fluid system. Shortly after, Guran and Plaut (1994b) studied the dynamics of a pinned-free pipe conveying fluid, additionally supported at the pinned end by a rotational spring, under an axial load acting at the free end. It was concluded

that flutter or divergence may arise, depending on the combination of the flow velocity and load. It ought to be mentioned here that the problem of a pipe conveying fluid with additional flexible supports at the upstream end is not wholly academic; long hanging tubulars used in hydrocarbon storage wells are one possible application; see, for example, Ratigan (2008).

An interesting problem which has perplexed researchers for nearly 30 years and continues to receive attention to this day from both fundamental and applied perspectives, is the dynamics of a cantilevered pipe *aspirating fluid*, i.e. where the pipe ingests fluid at the free end and conveys it towards the clamped end. Perhaps the first published research on this topic was by Païdoussis and Luu (1985), who conducted an analytical investigation of the system and concluded that, in the absence of damping, the aspirating pipe loses stability by flutter at infinitesimally low flow velocities, and it then regains stability at higher flow; this prediction was in clear contradiction to experimental investigations, in which *no* instability was observed; see Païdoussis (1998). From then on, several researchers revisited the problem, hoping to resolve this disagreement between theory and experiment. Païdoussis (1999) re-evaluated the analytical problem with a new assumption regarding the flow field at the intake (free end), concluding that no instability can occur. Later, Kuiper and Metrikine (2005) made some modifications to the analytical model and provided an explanation as to why flutter did not occur in the experiments. Almost concurrently, a theoretical reappraisal of the problem was undertaken by Païdoussis et al. (2005), considering some ideas originally proposed by Pramila (1992). Several new sets of experiments and a CFD-based numerical analysis were performed to provide further information about the problem (Kuiper et al., 2007; Kuiper and Metrikine, 2008; Giacobbi et al., 2008). Most recently, a paper has been published by Giacobbi et al. (2012), in which the dynamics of pipes aspirating fluid has thoroughly been studied by experimental, numerical and analytical methods; a comprehensive review of studies undertaken so far on this topic may also be found in that paper. To learn about some applications related to this problem, e.g. in ocean mining, the reader is referred to Païdoussis (1998) and papers by Xia et al. (2004) and Verichev et al. (2011).

Apart from numerous researches carried out on the linear dynamics of pipes conveying fluid, a great deal of remarkable work has also been done on the nonlinear dynamics of such systems. First of all, several appropriate sets of equations of motion have been put forward; among them, the work of Rousselet and Herrmann (1981), Lundgren et al. (1979), Bajaj et al. (1980), Ch'ng and Dowell (1979) and Semler et al. (1994), obtained via either a Newtonian or a Hamiltonian approach; also, the alternative approach based on the extended Lagrange equations proposed by Stangl et al. (2008) is worth mentioning. Special effort has also been made to generalize the analysis to cases of three-dimensional motions and to investigate various aspects of the nonlinear dynamics of *modified* systems; for example, pipes with intra-span springs or with an end-mass. Some of the early such studies have been reviewed briefly in Païdoussis and Li (1993) and in more detail in Païdoussis (1998); some more recent developments can also be found in reviews by Ibrahim (2010) and Païdoussis (2010).

Studying various aspects of dynamics of pipes conveying fluid is still today of great interest to researchers in the field of fluid–structure interactions. The often surprising dynamical behaviour displayed continues perplexing investigators and encourages them to do further studies. In fact, the current interest lies not only in nonlinear analysis of these systems, but also in linear analysis; applied problems also receive increasingly more attention. Some of very recent studies related to the subject of pipes conveying fluid can be found in the work of Ghayesh and Païdoussis (2010), Ghayesh et al. (2011, 2012), Hellum et al. (2013) and Firouz-Abadi et al. (2013).

In this paper, the equation of motion is derived for a pipe conveying fluid supported at both ends by linear translational and rotational springs. In the derivation, the effect of end-springs is appropriately incorporated in the equation of motion, rather than in the boundary conditions. The resulting *general* equation of motion in fact allows us to examine the dynamics of a pipe conveying fluid with any type of boundary conditions, either classical or non-classical, without any need to use different formulations for obtaining solutions. The present equation of motion is initially evaluated considering the case of a pipe with no fluid inside it, i.e. a beam, in Section 4.1. Then, in Section 4.2 and for the first time, the dynamics of a pinned-free pipe conveying fluid is studied.[2] As previously mentioned, since the dynamics of pipes conveying fluid with modifications at the downstream end has been studied sufficiently already, here we exclusively analyze cases in which springs are introduced at the upstream end of the pipe. Thus, in Section 4.3 the dynamics of a pinned-free pipe with a rotational spring at the pinned end is investigated, and in Section 4.4, a pipe supported at the upstream end by a translational and a rotational spring and free at the other is considered.

2. Definitions and preliminaries

2.1. Assumptions and the basic model

The simplest linear form of the equation of motion of a flexible pipe conveying fluid, performing planar motions, can be written as Païdoussis (1998)

$$EI\frac{\partial^4 w}{\partial x^4}+MU^2\frac{\partial^2 w}{\partial x^2}+2MU\frac{\partial^2 w}{\partial x\partial t}+(M+m)\frac{\partial^2 w}{\partial t^2}=0, \tag{1}$$

[2] To the best of authors' knowledge, the dynamics of a pipe conveying fluid with pinned-free boundary conditions, in the manner adopted in the present paper, has not previously been considered by others.

where EI is the flexural rigidity of the pipe, assumed to be constant along the pipe, M is the mass of fluid per unit length, flowing steadily with velocity U,[3] m is the mass of the pipe per unit length, w is the pipe deflection in the transverse direction, which is assumed to be small relative to the length of the pipe, i.e. $w/L \sim O(\epsilon)$, where $\epsilon \ll 1$; x and t are the axial coordinate and time, respectively (see Fig. 1(a)).

The first term in Eq. (1) represents the flexural restoring force; the second term is associated with the centrifugal forces generated as the fluid flows in curved portions of the pipe. The third term is related to Coriolis forces: the fluid flows longitudinally, while sections of the pipe rotate. The last term represents the inertial force of the fluid–pipe system.

The basic configuration (the classical configuration) shown in Fig. 1(a) can be generalized by considering flexible restraints at the ends of the pipe, as shown in Fig. 1(b). In the figure, K_0 and C_0 are, respectively, translational and rotational spring constants at $s=0$; K_L and C_L are the same quantities at $s=L$; s is the curvilinear coordinate along the centreline of the pipe. It is noted that the translational springs can only be deformed in the y-direction.

The equation of motion in the form given in Eq. (1) can be derived via either the Newtonian or the Hamiltonian approach; see, e.g., Benjamin (1961a), McIver (1973) and Païdoussis (1998). An alternative approach is to derive the equation of motion in the form of a set of ordinary differential equations via the extended version of the Lagrange equations (Stangl et al., 2008).

3. The equation of motion

In this paper, the Hamiltonian approach is used to derive the equation of motion. First, we consider the principle of virtual work for the so-called *closed* system which, by definition, has a constant mass and constitutes particles of fixed identity. The system occupies a moving region of space $V_c(t)$ bounded by the surface $B_c(t)$ across which there is no mass transport. The density of particles and their associated velocity at position $\boldsymbol{r}$ and time t are represented, respectively, by ρ and $\boldsymbol{u}$. The principle of virtual work for such a system can therefore be written as

$$\delta\mathcal{L}_c+\delta\mathcal{W}-\frac{\mathrm{D}}{\mathrm{D}t}\iiint_{V_c}\rho(\boldsymbol{u}.\delta\boldsymbol{r})\,\mathrm{d}V=0, \tag{2}$$

where $\mathcal{L}_c=\mathcal{T}_c-\mathcal{V}_c$ is the Lagrangian of the system, $\mathcal{T}_c$ and $\mathcal{V}_c$ being the kinetic and potential energies of the particles within the closed region $V_c(t)$; $\delta\mathcal{W}$ is the virtual work of the external forces due to virtual displacements of the pipe; $\mathrm{D}(\,)/\mathrm{D}t$ is the material derivative following a particle; hence, $\boldsymbol{u}=\mathrm{D}\boldsymbol{r}/\mathrm{D}t$.

By integrating Eq. (2) with respect to time between instants t_1 and t_2, the last term vanishes due to the fact that $\delta\boldsymbol{r}(t_1)=\delta\boldsymbol{r}(t_2)=0$, and the familiar form of Hamilton's principle is then obtained.

3.1. Hamilton's principle for an open system

Next, the principle given in Eq. (2) is extended to a system with changing mass, where mass, momentum and energy transfer can take place across the boundaries. The system in this case is usually referred to as an *open system* or a *control volume*. The principle of virtual work for such an *open system* may be written as

$$\delta\mathcal{L}_o+\delta\mathcal{W}+\iint_{B_o(t)}\rho(\boldsymbol{u}.\delta\boldsymbol{r})(\boldsymbol{V}-\boldsymbol{u}).\boldsymbol{n}\,\mathrm{d}S-\frac{\mathrm{d}}{\mathrm{d}t}\iiint_{V_o(t)}\rho(\boldsymbol{u}.\delta\boldsymbol{r})\,\mathrm{d}V=0, \tag{3}$$

where $\mathcal{L}_o$ and $\mathcal{W}$ are, respectively, the Lagrangian and the virtual work associated with the open system; $\boldsymbol{V}$ is the velocity of boundary $B_o(t)$ of control volume $V_o(t)$, and $\boldsymbol{n}$ is the outward normal; see McIver (1973) for details.

Hamilton's principle for a system of changing mass may be deduced from Eq. (3) as[4]

$$\delta\int_{t_1}^{t_2}\mathcal{L}_o\,\mathrm{d}t+\int_{t_1}^{t_2}\delta\mathcal{H}\,\mathrm{d}t=0, \tag{4}$$

where

$$\delta\mathcal{H}=\delta\mathcal{W}+\iint_{B_o(t)}\rho(\boldsymbol{u}.\delta\boldsymbol{r})(\boldsymbol{V}-\boldsymbol{u}).\boldsymbol{n}\,\mathrm{d}S, \tag{5}$$

in which the last integral may be thought of as a virtual momentum transport across the open surface $B_o(t)$.

[3] The flow in the pipe is fully developed turbulent; therefore, a uniform velocity profile assumption (a plug flow model) is reasonable.

[4] In a very recent paper by Casetta and Pesce (2013), a more general form than McIver's (1973) statement of Hamilton's principle for open systems of changing mass or non-material volumes is derived. This derivation, in addition to the flux of momentum through the control surface, which has also been considered in McIver's (1973) expression, takes into account the flux of kinetic energy transported through the control surface. This new form of Hamilton's principle is also consistent with the Lagrange equations for a non-material volume, as formulated by Irschik and Holl (2002). Despite all that, McIver's (1973) statement of Hamilton's principle can still be used, at least for systems of pipes conveying incompressible fluid. McIver's assumption that "the generalized co-ordinates of the pipe characterize the system and a generalized virtual displacement does not (in this case) induce a virtual displacement of the fluid relative to the pipe" (see McIver, 1973, p. 259) would reduce the expression proposed by Casetta and Pesce (2013) to the expression obtained by him. Mathematically speaking, the assumption made by McIver may finally result in letting $\delta\boldsymbol{p}=\delta\boldsymbol{r}$ in equation (31) of Casetta and Pesce (2013), by which the flux of kinetic energy through the control surface vanishes. It is noted here that $\delta\boldsymbol{p}$ and $\delta\boldsymbol{r}$ are the virtual displacement distributions associated with the material and fictitious particles, respectively.

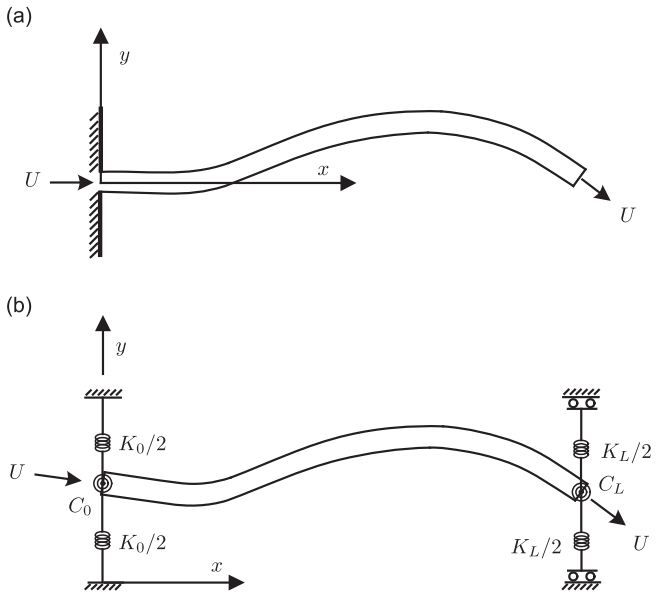

Fig. 1. (a) A cantilevered pipe conveying fluid (basic configuration); (b) a pipe conveying fluid with flexible restraints at the ends (generalized configuration); K_0 and C_0 are, respectively, translational and rotational springs at $s=0$; K_L and C_L are the same quantities at $s=L$; s is the curvilinear coordinate along the centreline of the pipe.

3.2. The extended virtual work for a pipe flexibly restrained at its ends

Now, consider Fig. 2 which shows one possible configuration for a pipe conveying fluid and flexibly restrained at the ends. As shown in the figure, a short ($d \ll L$), rigid, massless funnel of bell-mouthed shape is attached to the inlet of the pipe via an elastic coupling; this serves to ensure that flow enters the pipe smoothly, with no significant loss associated with the *vena contracta* effect.[5] All motions of the pipe are supposed to take place in a horizontal plane, wherein the x- and y-axes also lie. The mean flow velocity just before the funnel is $v\boldsymbol{i}$, and it becomes $U\boldsymbol{\tau}$ inside the pipe, where $\boldsymbol{i}$ is the unit vector in the x-direction, and $\boldsymbol{\tau}$ is the unit tangential vector along the pipe.

If the funnel and the coupling with the fluid within are labeled as *system1* and the pipe with the fluid in it *system2*, it is customary to use the linear momentum equation to find the forces exerted on system1 by system2; then replacing system1 with the forces (reactions) acting on system2, with the flow conditions exactly as if system1 were in place. This has fully been undertaken in Appendix A; accordingly, the forces which should be placed at the inlet of system2 ($s=0$ or $x=0$) are written as

$$\begin{aligned} F_x^{(2)} &= -[-F_{x,s}^{(1)} + p_e^{(1)}A\ \cos\chi|_{s=0} - p_i^{(1)}A_i^{(1)} + \rho AU^2\ \cos\chi|_{s=0} - \rho A_i^{(1)}v^2], \\ F_y^{(2)} &= -[p_e^{(1)}A\ \sin\chi|_{s=0} + \rho AU^2\ \sin\chi|_{s=0} + \rho AU\dot{w}|_{s=0}], \end{aligned} \tag{6}$$

where $F_x^{(2)}$ and $F_y^{(2)}$ are the forces acting on system2, respectively in the x- and y-directions; $F_{x,s}^{(1)}$ is the force exerted on system1, in the x-direction, due to the presence of the supports; p stands for the hydrostatic pressure measured above the atmospheric; χ is the angle between the pipe centreline and the x-axis; subscripts i and e refer to the inlet and exit, respectively, and superscripts (1) and (2) denote quantities associated with system1 and system2, respectively; also, $(\dot{}) = \partial(\ )/\partial t$.

As flow leaves system1, it enters system2 with velocity $U\boldsymbol{\tau}$, i.e. the flow enters the pipe tangential to its centreline, and static pressure $p_i^{(2)}$ where $p_i^{(2)} = p_e^{(1)}$. Considering these conditions along with forces $F_x^{(2)}$ and $F_y^{(2)}$, $\delta\mathcal{H}$, as introduced in Eq. (5), may be written as

$$\begin{aligned} \delta\mathcal{H} = {} & \delta\overline{\mathcal{W}} + (F_x^{(2)} + p_i^{(2)}A\ \cos\chi|_{s=0})\delta x|_{s=0} + (F_y^{(2)} + p_i^{(2)}A\ \sin\chi|_{s=0})\delta w|_{s=0} \\ & + \iint_{S_i^{(2)}} [\rho(U\boldsymbol{\tau} + \dot{x}\boldsymbol{i} + \dot{w}\boldsymbol{j}) \cdot (\delta x\boldsymbol{i} + \delta w\boldsymbol{j})(-U\boldsymbol{\tau}) \cdot (-\boldsymbol{\tau})]_{s=0}\, \mathrm{d}S \\ & + \iint_{S_e^{(2)}} [\rho(U\boldsymbol{\tau} + \dot{x}\boldsymbol{i} + \dot{w}\boldsymbol{j}) \cdot (\delta x\boldsymbol{i} + \delta w\boldsymbol{j})(-U\boldsymbol{\tau}) \cdot (\boldsymbol{\tau})]_{s=L}\, \mathrm{d}S, \end{aligned} \tag{7}$$

[5] As flow enters the pipe through the entrance, flow separation in the pipe causes the main stream to contract to a minimum diameter, constituting the *vena contracta*. The turbulence created by the expansion of the stream after it passes the vena contracta is recognized as the primary reason for the entrance loss (Daugherty and Franzini, 1965; White, 2008).

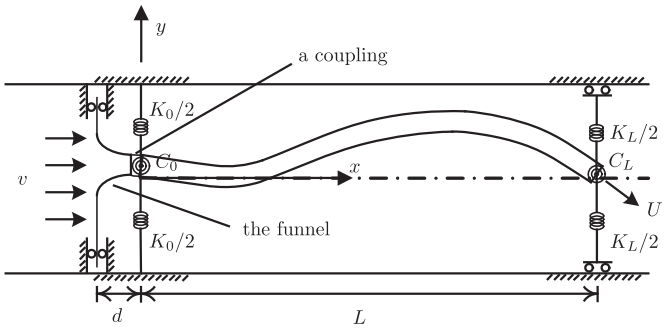

Fig. 2. One possible configuration for a pipe conveying fluid with flexible restraints at the ends; the funnel or bell-mouthed intake is assumed to be short ($d \ll L$), rigid and massless and to be attached to the pipe inlet via an elastic coupling; v is the mean flow upstream velocity, and U is the flow velocity in the pipe. The upstream end of the pipe does not move in the x-direction, while its downstream end is free to move in that direction.

where $\dot{x}$ is the velocity of any point on the pipe in the x-direction, and $\delta\overline{\mathcal{W}}$ is the virtual work associated with forces other than the pressure forces. The above equation has been obtained by considering the fact that all boundaries of system2 (the pipe), except for the inlet, are surrounded by the atmosphere.

Letting $\delta x|_{s=0} = 0$ and $\dot{x}|_{s=0} = 0$,[6] and using the expression for $F_y^{(2)}$, given in Eq. (6), Eq. (7) may be simplified to

$$\delta\mathcal{H} = \delta\overline{\mathcal{W}} - MU^2(x'_L\delta x_L + w'_L\delta w_L) - MU(\dot{x}_L\delta x_L + \dot{w}_L\delta w_L), \tag{8}$$

where the subscript L signifies the quantity concerned at $s=L$; also, $(\,)' = \partial(\,)/\partial s$.

3.3. Kinetic and potential energies of the fluid–pipe system

The total kinetic energy of the system can be written by considering a small segment of the pipe with the fluid inside

$$\mathcal{T} = \frac{1}{2}\int_0^L m\boldsymbol{V}_p\cdot\boldsymbol{V}_p\,\mathrm{d}s + \frac{1}{2}\int_0^L M(U\boldsymbol{\tau}+\boldsymbol{V}_p)\cdot(U\boldsymbol{\tau}+\boldsymbol{V}_p)\,\mathrm{d}s, \tag{9}$$

where $\boldsymbol{V}_p = \dot{x}\boldsymbol{i}+\dot{y}\boldsymbol{j}$ is the velocity of the pipe element, and $U\boldsymbol{\tau}+\boldsymbol{V}_p$ is the velocity of the fluid element.

The variational operation on $\int_{t_1}^{t_2}\mathcal{T}\,\mathrm{d}t$ and several simplifications afterwards lead to

$$\begin{aligned}\delta\int_{t_1}^{t_2}\mathcal{T}\,\mathrm{d}t = &-\int_{t_1}^{t_2}\int_0^L[(m+M)\ddot{x}+2MU\dot{x}']\delta x\,\mathrm{d}s\,\mathrm{d}t - \int_{t_1}^{t_2}\int_0^L[(m+M)\ddot{w}+2MU\dot{w}']\delta w\,\mathrm{d}s\,\mathrm{d}t\\ &+MU\int_{t_1}^{t_2}[\dot{x}_L\delta x_L+\dot{w}_L\delta w_L]\,\mathrm{d}t - MU\int_{t_1}^{t_2}[\dot{x}_0\delta x_0+\dot{w}_0\delta w_0]\,\mathrm{d}t,\end{aligned} \tag{10}$$

where subscripts 0 and L refer to $s=0$ and $s=L$, respectively.

The potential energy of the system, in the absence of gravity, comprises the strain energy of the pipe and the elastic energy of the springs:

$$\mathcal{V} = \frac{1}{2}\int_0^L EI\bar{\kappa}^2\,\mathrm{d}s + \frac{1}{2}K_0w_0^2 + \frac{1}{2}C_0w_0'^2 + \frac{1}{2}K_Lw_L^2 + \frac{1}{2}C_Lw_L'^2, \tag{11}$$

where $\bar{\kappa}$ is the curvature of the neutral axis of the pipe; for a pipe with negligible axial strain this is $\bar{\kappa} = w''/(1-w'^2)^{1/2}$ (see Semler et al., 1994 for details).

Considering only linear terms in the expression of curvature, the variational form of $\int_{t_1}^{t_2}\mathcal{V}\,\mathrm{d}t$ may be written as

$$\delta\int_{t_1}^{t_2}\mathcal{V}\,\mathrm{d}t = \int_{t_1}^{t_2}\int_0^L EIw''''\delta w\,\mathrm{d}s\,\mathrm{d}t + \int_{t_1}^{t2}[K_0w_0\delta w_0 + C_0w'_0\delta w'_0 + K_Lw_L\delta w_L + C_Lw'_L\delta w'_L]\,\mathrm{d}t; \tag{12}$$

see Appendix B for more details.

3.4. Relationship between δx and δw

Following the procedure described in Semler et al. (1994), we can find the relationship between the virtual displacements δx and δw. It is noted that, unlike the case considered there (a cantilevered pipe), for the case treated in

[6] It is assumed that the upstream end of the pipe does not move in the x-direction.

this study δw_0 is not necessarily zero. Thus, this relationship, in linear form, is

$$\delta x = w_0'\delta w_0 - w'\delta w + \int_0^s w''\delta w \, ds. \tag{13}$$

Then, from the above equation one can write

$$\delta x_L = w_0'\delta w_0 - w_L'\delta w_L + \int_0^L w''\delta w \, ds. \tag{14}$$

3.5. The equation of motion and the boundary conditions

The equation of motion can be obtained by substituting Eqs. (8), (10), (12) and (14) in Eq. (4) and performing some manipulations (see Appendix B):

$$\begin{aligned}&[EIw'''' + MU^2w'' + 2MU\dot{w}' + (m+M)\ddot{w}]\delta w + MU[\dot{w} + Uw']\delta w\bar{\delta}(s)\\ &\quad + [K_0 w\delta w + C_0 w'\delta w']\bar{\delta}(s) + [K_L w\delta w + C_L w'\delta w']\bar{\delta}(s-L) = 0,\end{aligned} \tag{15}$$

where $\bar{\delta}(s)$ is the Dirac delta function.

As one can see in Eq. (15) (for arbitrary variations δw and $\delta w'$ with $s \simeq x$), the basic form of the equation of motion, Eq. (1), has been modified by the presence of fluid momentum transport into the pipe (second group of terms in Eq. (15)) and translational and rotational springs at the ends of the pipe (last two groups of terms in the above equation). It is also noted that only linear terms of $O(\epsilon)$ have been retained in the equation of motion, while higher order terms have been ignored.

Since the effect of the end-springs has suitably been considered in the potential energy of the system and forces due to the fluid momentum transport to the pipe have been treated in the extended form of virtual work, the boundary conditions of the system will simply be

$$EIw''' = EIw'' = 0 \quad \text{at } s = 0 \text{ and } s = L, \tag{16}$$

which are the boundary conditions for a free–free beam undergoing transverse vibrations (see Appendix B for details).

The equation of motion and boundary conditions may be rendered dimensionless through the use of[7]

$$\xi = \frac{x}{L}, \quad \eta = \frac{w}{L}, \quad \tau = \left(\frac{EI}{M+m}\right)^{1/2}\frac{t}{L^2}. \tag{17}$$

The dimensionless form of Eq. (15) is then

$$[\eta'''' + u^2\eta'' + 2\beta^{1/2}u\dot{\eta}' + \ddot{\eta}]\delta\eta + u[\beta^{1/2}\dot{\eta} + u\eta']\delta\eta\bar{\delta}(\xi) + [\kappa_0\eta\delta\eta + \kappa_0^*\eta'\delta\eta']\bar{\delta}(\xi) + [\kappa_1\eta\delta\eta + \kappa_1^*\eta'\delta\eta']\bar{\delta}(\xi-1) = 0, \tag{18}$$

and the boundary conditions are

$$\eta''' = \eta'' = 0 \quad \text{at } \xi = 0 \text{ and } \xi = 1, \tag{19}$$

where $\dot{(\,)} = \partial(\,)/\partial\tau$ and $(\,)' = \partial(\,)/\partial\xi$, in which the following dimensionless system parameters have appeared:

$$\begin{aligned}&u = \left(\frac{M}{EI}\right)^{1/2}LU, \quad \beta = \frac{M}{M+m},\\ &\kappa_0 = \frac{K_0L^3}{EI}, \quad \kappa_0^* = \frac{C_0L}{EI}, \quad \kappa_1 = \frac{K_LL^3}{EI}, \quad \kappa_1^* = \frac{C_LL}{EI}.\end{aligned} \tag{20}$$

Eq. (18) can be transformed into a set of second-order ordinary differential equations using Galerkin's method; thus, we let

$$\eta(\xi,\tau) = \sum_{j=1}^{N}\phi_j(\xi)q_j(\tau), \tag{21}$$

where $\phi_j(\xi)$ are the free–free Euler–Bernoulli beam eigenfunctions, used here as a suitable set of base functions[8]; $q_j(\tau)$ are the corresponding generalized coordinates and N denotes the number of eigenfunctions (modes) used in the analysis.

The equation of motion in discretized form is obtained by applying the Galerkin method to Eq. (18):

$$[\mathbb{M}]\{\ddot{\mathbf{q}}\} + [\mathbb{C}]\{\dot{\mathbf{q}}\} + [\mathbb{K}]\{\mathbf{q}\} = 0, \tag{22}$$

[7] We also use $s \simeq x$, as it is assumed that axial strain is negligible, i.e. the centreline of the pipe is inextensible, and only linear terms are retained in the derivations.

[8] For a suitable set of eigenfunctions for a free–free Euler–Bernoulli beam, the reader may refer to Kheiri et al. (2013a), or alternatively, to Meirovitch (1967).

where $\mathbf{q}$ is the vector of the generalized coordinates; $\mathbb{M}$, $\mathbb{C}$ and $\mathbb{K}$ correspond to the mass, damping and stiffness matrices, respectively, the elements of which, M_{ij}, C_{ij} and K_{ij}, may be written as

$$M_{ij}=\delta_{ij},\quad C_{ij}=2\beta^{1/2}ub_{ij}+\beta^{1/2}u\phi_i(0)\phi_j(0),$$
$$K_{ij}=\lambda_j^4\delta_{ij}+u^2c_{ij}+u^2\phi_i(0)\phi_j'(0)+\kappa_0\phi_i(0)\phi_j(0)+\kappa_0^*\phi_i'(0)\phi_j'(0)+\kappa_1\phi_i(1)\phi_j(1)+\kappa_1^*\phi_i'(1)\phi_j'(1), \tag{23}$$

in which the orthonormality of the eigenfunctions, i.e. $\int_0^1 \phi_i\phi_j\,\mathrm{d}\xi=\delta_{ij}$, with δ_{ij} being Kronecker's delta, and the fact that $\phi_j''''=\lambda_j^4\phi_j$, λ_j being the jth dimensionless eigenvalue of the beam, have been utilized; b_{ij} and c_{ij} are defined by

$$b_{ij}=\int_0^1 \phi_i\phi_j'\,\mathrm{d}\xi,\quad c_{ij}=\int_0^1 \phi_i\phi_j''\,\mathrm{d}\xi. \tag{24}$$

The above integrals can either be computed numerically or found analytically. The analytical expressions are more desirable for obvious reasons. Some techniques for the analytical evaluation of b_{ij} and c_{ij} are presented in Appendix C.

3.6. The energy transfer between the fluid and the pipe

The rate of work done on the pipe by the fluid dynamic forces, as well as the end-springs, in the course of periodic motions is

$$\frac{\mathrm{d}W}{\mathrm{d}t}=-\int_0^L \frac{\partial w}{\partial t}M\left\{\frac{\partial}{\partial t}+U\frac{\partial}{\partial x}\right\}\left[\frac{\partial w}{\partial t}+U\frac{\partial w}{\partial t}\right]\mathrm{d}x-MU\left[U\frac{\partial w_0}{\partial x}+\frac{\partial w_0}{\partial t}\right]\left(\frac{\partial w_0}{\partial t}\right)+\left(\frac{\mathrm{d}W}{\mathrm{d}t}\right)_s, \tag{25}$$

where the integrand is basically the time-rate of change of fluid momentum in the y-direction, i.e. the force exerted on the fluid, multiplied by the velocity of the pipe in the transverse direction; the second term is the rate of work done by the concentrated fluid-related force (the second expression in parentheses in Eq. (7)) acting at the upstream end of the pipe; $(\mathrm{d}W/\mathrm{d}t)_s$ is the rate of work done by the end-springs.

Hence, the work done on the pipe over a cycle of periodic oscillation of period T is

$$\Delta W=-M\int_0^T\int_0^L \frac{\partial w}{\partial t}\left\{\frac{\partial}{\partial t}+U\frac{\partial}{\partial x}\right\}\left[\frac{\partial w}{\partial t}+U\frac{\partial w}{\partial t}\right]\mathrm{d}x\,\mathrm{d}t-MU\int_0^T\left[U\frac{\partial w_0}{\partial x}+\frac{\partial w_0}{\partial t}\right]\left(\frac{\partial w_0}{\partial t}\right)\mathrm{d}t, \tag{26}$$

in which the fact that the work done by the end-springs, over a cycle, is zero has been used.

Eq. (26) can be simplified after integration by parts, as well as through use of periodicity properties, such as $(\partial w/\partial t)|_0^T=0$ and $(\partial w/\partial x)|_0^T=0$. Thus,

$$\Delta W=-MU\int_0^T\left[\left(\frac{\partial w}{\partial t}\right)_L^2+U\left(\frac{\partial w}{\partial t}\right)_L\left(\frac{\partial w}{\partial x}\right)_L\right]\mathrm{d}t, \tag{27}$$

which means that the work done on the pipe over a cycle of periodic motions is dependent on the lateral velocity and slope of the pipe at $x=L$, as well as on MU. It is also interesting to see that Eq. (27) is the same as the equation obtained for the work done on a cantilevered pipe conveying fluid (cf. equation (3.11) in Païdoussis, 1998). It should be remarked that the fact that there are no $(\partial w/\partial t)_0$, $(\partial w/\partial x)_0$ terms left in (27) is due to the artifice of the upstream bell-mouthed massless intake (Fig. 2).

From Eq. (27) it is seen that, when U is small, the first term in the integrand predominates, and hence $\Delta W<0$, i.e. the energy transfer from the fluid to the pipe is negative and therefore vibrations about the stable equilibrium are damped. On the other hand, at sufficiently high U, ΔW may become positive, i.e. the pipe will gain energy from the flow, and the vibrations will be amplified, provided that over most of the cycle $(\partial w/\partial x)_L$ and $(\partial w/\partial t)_L$ have opposite signs. This suggests that, in the course of oscillations, the pipe must perform a sort of *dragging*, *lagging* motion, as observed by Benjamin (1961b), Gregory and Païdoussis (1966b) and others.

Eq. (27) could also be obtained directly from the extended virtual work of an open system (second term on the right-hand of Eq. (5), and in the simplified form, the second and third terms on the right-hand of Eq. (8)), as developed by Benjamin (1961a) and recalled by Semler et al. (1994).

The dimensionless form of Eq. (27) may be written as

$$\Delta\tilde{W}=-u\int_0^{\tilde{T}}\left[\beta^{1/2}\left(\frac{\partial\eta}{\partial\tau}\right)_1^2+u\left(\frac{\partial\eta}{\partial\tau}\right)_1\left(\frac{\partial\eta}{\partial\xi}\right)_1\right]\mathrm{d}\tau, \tag{28}$$

in which $\Delta\tilde{W}=\Delta W/(EI/L)$ and $\tilde{T}$ are dimensionless energy transfer and period, respectively.

4. Numerical solutions and discussion

The normal way for studying the dynamical behaviour of a linear system is by obtaining the eigenvalues or equivalently eigenfrequencies[9] of the system, as a system parameter, for example the flow velocity, is varied. The evolution of the

[9] If for example, $\tilde{\lambda}_j$ is the jth eigenvalue and ω_j is the jth eigenfrequency of the system ($\tilde{\lambda}_j$ and ω_j are generally complex-valued quantities), one can write: $\tilde{\lambda}_j=\mathrm{i}\omega_j$, where $\mathrm{i}=\sqrt{-1}$.

generally complex eigenfrequencies can be presented as an *Argand* diagram, in which the abscissa and the ordinate correspond to the real and imaginary parts of the eigenfrequencies ($\mathrm{Re}(\omega)$ and $\mathrm{Im}(\omega)$), respectively. It is recalled that $\mathrm{Re}(\omega)$ is the dimensionless oscillation frequency, and $\mathrm{Im}(\omega)$ is related to damping, i.e. the damping ratio is $\zeta = \mathrm{Im}(\omega)/\mathrm{Re}(\omega)$. As a result, $\mathrm{Im}(\omega) > 0$ indicates stability, while $\mathrm{Im}(\omega) < 0$ means instability; more specifically, instability materializes by the crossing of the eigenfrequency locus from the positive to the negative half-plane in the Argand diagram (see Païdoussis, 1998, for details).

In this paper, to be able to present the results in Argand diagrams, Eq. (22) should first be transformed to first-order or state-space form; this can easily be done by letting $\dot{\mathbf{q}} = \overline{\mathbf{u}}$; then, several eigenvalue-problem solvers found in commercial software, such as MATLAB and Maple, can be used to obtain the eigenvalues and thence eigenfrequencies of the system.

However, before performing any analysis on the flexibly end-restrained pipe conveying fluid system, it may well be justifiable, as the first step, to examine a simplified version of the original system. Therefore, a flexibly end-restrained pipe with no fluid inside it, i.e. a beam with flexible end-conditions, is examined first. Several numerical studies can be carried out on this system to assess the validity of the mathematical modelling, presented in this study; this is the subject of the next section.

4.1. An Euler–Bernoulli beam with flexible end-conditions

As just mentioned, a preliminary test of the mathematical model developed in this paper can be done by analyzing a beam, supported at both ends by translational and rotational springs. It is known that by properly setting the end-spring constants to zero or infinity, the boundary conditions of the system may come very close to the classical ones; e.g., clamped-free boundary conditions, if $\kappa_0, \kappa_0^* \to \infty$ and $\kappa_1 = \kappa_1^* = 0$, and pinned–pinned boundary conditions, if $\kappa_0, \kappa_1 \to \infty$ and $\kappa_0^* = \kappa_1^* = 0$.

Some numerical calculations have been made, in which the first five eigenvalues have been obtained for a beam with classical boundary conditions, such as pinned-free, clamped-free, pinned–pinned, clamped–pinned and clamped–clamped.[10] The boundary conditions were imposed by setting the end-spring constants to appropriate values, i.e. either zero or infinity. The results show very good agreement with values found in vibration books, for example Rao (2007); the maximum difference is found to be $\simeq 2.24\%$.

Several numerical comparisons have also been made, in which the eigenvalues ($\tilde{\lambda}_j$'s) for free vibration of the beam, obtained via the present model, are compared with the results obtained by Li (2000), for various combinations of springs and spring constants ranging from low to high values. In these calculations, 40 modes, i.e. $N=40$, are used in the Galerkin expansion, and 100 digits are used to compute the matrices.

Thus, consider a case in which, as originally done by Li (2000), a pinned–pinned beam is additionally supported by a very stiff rotational spring at $\xi=0$, let us say $\kappa_0^* = 10^{10}$, and a rotational spring with stiffness κ_1^* at $\xi=1$; κ_1^* is varied from 0 to 10^{10}, in the first limit corresponding to a clamped–pinned beam, while in the other limit to a clamped–clamped beam. Table 1 gives the first four (four lowest) dimensionless eigenvalues (for this case, they are strictly: $\tilde{\lambda}_j/\pi$, where $j=1\ldots4$) of the system, obtained using the present model, for various values of κ_1^*. The values in this table can be compared with those presented in Table 1 of Li (2000). The two sets of results are generally in good agreement; to be more specific, the maximum relative error between the two sets is $\simeq 2.17\%$. It is also noted that to come close to pinned–pinned boundary conditions, we have let $\kappa_0 = \kappa_1 = 10^{10}$.

In the second test case, the first (lowest) eigenvalue ($\tilde{\lambda}_1$) of a pinned-free beam additionally supported at the pinned end by a rotational spring of stiffness κ_0^* and at the free end by a translational one of stiffness κ_1 is obtained for various values of κ_0^* and κ_1. The corresponding values are given in Table 2 and can be compared with the values given in Table 4 of Li (2000). The values obtained here and those given in Li (2000) are again very close, with a maximum difference of $\simeq 1\%$.

The last set of results of this type is obtained for a beam supported by relatively very flexible translational springs at both ends ($\kappa_0 = \kappa_1 = 1$) and rotational springs of stiffness κ_0^* and κ_1^*, respectively at $\xi=0$ and $\xi=1$; κ_0^* and κ_1^* are assumed to be equal and are varied from 0.01 to 100. The first five eigenvalues of the system are given in Table 3, and they can be compared with the values given in Table 5 of Li (2000). The difference between the two sets of results in this case also is negligible, the maximum of which is $\simeq 1\%$.

4.2. Dynamics and stability of a pinned-free pipe conveying fluid

The dynamics of pipes conveying fluid with various classical boundary conditions, such as clamped-free, pinned–pinned and clamped–clamped has been the subject of many studies so far. However, the dynamics of the system with pinned-free boundary conditions has received virtually no attention to-date. The purpose of this section is to investigate the dynamical behaviour of a pipe conveying fluid pinned at the upstream end and free at the other.

[10] Obviously, in these cases and in the cases to be discussed after in this section, since there is no damping present in the system, the eigenvalues will only have an imaginary component.

Table 1
The first four dimensionless eigenvalues (divided by π, i.e. $\tilde{\lambda}_j/\pi,\ j=1..4$) for a pinned–pinned beam additionally constrained by a very stiff rotational spring at $\xi=0$ and a rotational spring of stiffness κ_1^* at $\xi=1$ ($\kappa_0=\kappa_0^*=\kappa_1=10^{10}$, in this case). For numerical comparison, see Table 1 of Li (2000).

Mode	$\kappa_1^*=0$	$\kappa_1^*=1$	$\kappa_1^*=10$	$\kappa_1^*=100$	$\kappa_1^*=10^{10}$
1	1.26311	1.30018	1.43100	1.52199	1.53835
2	2.27406	2.29490	2.40206	2.52516	2.55309
3	3.28494	3.29981	3.39067	3.53674	3.57731
4	4.29625	4.30759	4.38444	4.54419	4.59751

Table 2
The first dimensionless eigenvalue ($\tilde{\lambda}_1$) for a pinned-free beam additionally constrained by a rotational spring of stiffness κ_0^* at $\xi=0$ and a translational spring of stiffness κ_1 at $\xi=1$ ($\kappa_0=10^{10}$, $\kappa_1^*=0$). For numerical comparison, see Table 4 of Li (2000).

κ_0^*	κ_1		
	0.01	1	100
0.01	0.4948	1.3134	2.9901
1	1.2546	1.5373	3.1094
100	1.8771	2.0104	3.6408

First, consider the equation of motion of a pipe conveying fluid, in its simplest form as given in Eq. (1), which in the dimensionless form becomes

$$\eta''''+u^2\eta''+2\beta^{1/2}u\dot{\eta}'+\ddot{\eta}=0. \tag{29}$$

If we neglect the time-dependent terms in the above equation, the following general static solution is obtained:

$$\eta(\xi)=A_1+A_2\xi+A_3\ \sin(u\xi)+A_4\ \cos(u\xi), \tag{30}$$

which, after applying the boundary conditions, i.e. $\eta(0)=\eta''(0)=\eta''(1)=\eta'''(1)=0$, and some other manipulations, becomes

$$\eta(\xi)=A_2\xi, \tag{31}$$

with no limiting condition for u, i.e. valid for any $u\geq 0$; $u=0$ is also a possible trivial solution to Eq. (30).

Thus, an infinite number of equilibrium configurations in the form of straight lines, all originating from the pinned end, appear. This suggests that the linear system is *neutrally* stable, i.e. if the system is perturbed, the perturbations will decay; the system, however, will not return to its original state, but it goes into another stable state.

The accuracy of the above statement is tested by performing stability analysis of the complete form of the equation of motion (Eq. (29)). One approach would be to first use the Galerkin method to discretize Eq. (29) and then to cast it in first-order form which could be solved numerically via standard eigenvalue-problem solvers. However, some time-domain solutions based on a central finite difference scheme are obtained here to investigate the stability of the system. For details on this scheme, refer to Kheiri et al. (2013c) and Sugiyama and Kawagoe (1975).

Fig. 3 shows the dynamics of the system for $\beta=0.2$ for several values of dimensionless flow velocity u, i.e. $u=1.0$, 3.0 and 7.0. The initial shape of the pipe is considered to be $\eta(\xi,0)=0.01\ \sin(\pi\xi/2)$, via which the final configuration of the pipe, after the transition, is obtained for each value of u, as given by the full lines in Fig. 3(a). The time history of the displacement of the pipe at its free end ($\xi=1.0$) is shown in Fig. 3(b) for the same three values of u. As seen in Fig. 3(a), the pipe finally takes on a stationary rigid-body form with no noticeable flexure; in other words, the pipe stretches along a straight line and has the form $\eta=A\xi$, where A varies only with u, similar to what was found in Eq. (31). In fact, the pipe with the new configuration can be regarded as being in undisturbed equilibrium, only slightly rotated about an axis perpendicular to the plane in which the oscillations occur. Hence, one may conclude that the system is *neutrally* stable, at least up to $u=7.0$, i.e. it only takes up another static equilibrium (stable) configuration without experiencing any type of instability.

However, at higher flow velocities ($u>7.0$ for the above-mentioned system), the system undergoes a dynamic instability in the form of a single-mode flutter. This can clearly be observed from Fig. 4, which shows in an Argand diagram the evolution of the first three dimensionless eigenfrequencies of the system,[11] ω, as a function of u (the numerals printed along each locus). As seen, for approximately $u<6.5$, flow induces damping in all modes of the system, i.e. $\mathrm{Im}(\omega)>0$; thus, any perturbation dies out, and the system remains stable; strictly speaking, *neutrally* stable. However, for higher u, $\mathrm{Im}(\omega)$ in the third mode of the system gradually diminishes and eventually becomes negative at $u=u_{cr}\simeq 7.34$, where the system loses stability via a Hopf bifurcation leading to the third-mode flutter. The rest of modes however, remain stable up to the maximum flow velocity considered here ($u_{\max}=10.0$). In fact, the first mode has two branches; one of them remains always

[11] The fourth mode is shown only partially.

Table 3
The first five dimensionless eigenvalues ($\tilde{\lambda}_j$, $j=1..5$) for a beam constrained by relatively very flexible translational springs at both ends ($\kappa_0=\kappa_1=1$) and torsional springs of stiffness κ_0^* and κ_1^*, respectively, at $\xi=0$ and $\xi=1$. For numerical comparison, see Table 5 of Li (2000).

Mode	$\kappa_0^*=\kappa_1^*$		
	0.01	1	100
1	1.18430	1.18565	1.18838
2	1.57924	2.23684	3.17414
3	4.75289	5.06576	6.29052
4	7.85988	8.07867	9.42842
5	10.99893	11.16269	12.57350

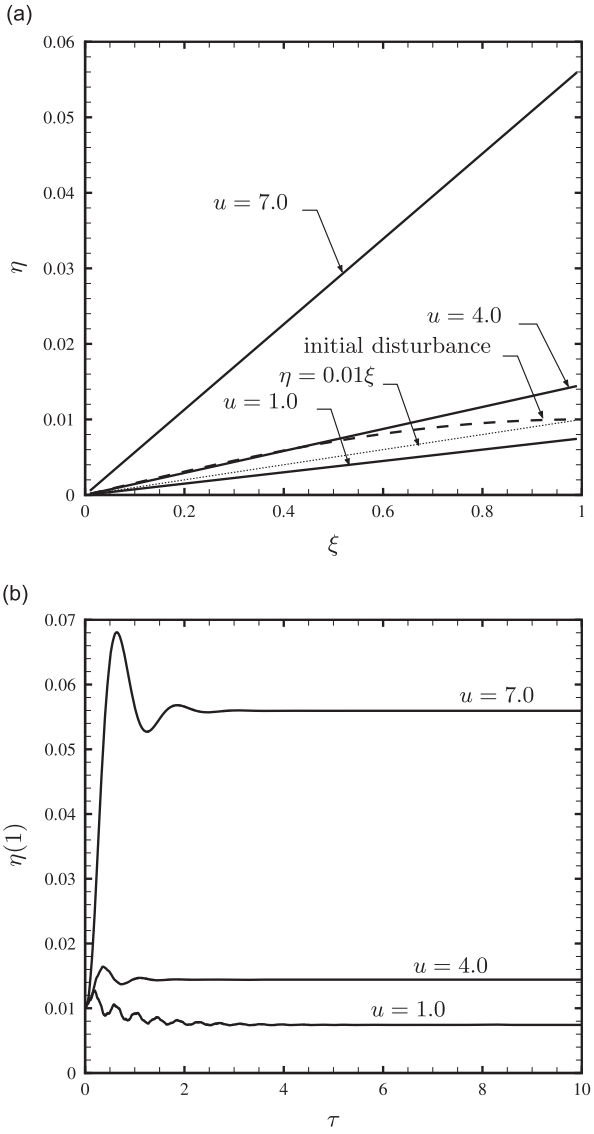

Fig. 3. The subcritical dynamics of a pinned-free pipe conveying fluid with an initial disturbance of $\eta(\xi,0)=0.01\sin(\pi\xi/2)$ and $\beta=0.2$: (a) the post-transient configuration of the pipe, and (b) the time history of the displacement of the pipe at $\xi=1$, for $u=1.0$, 4.0 and 7.0.

stationary at the origin; the second one, on the other hand, evolves exclusively on the positive Im(ω)−axis, as shown by arrows in the figure. The second mode also diminishes with increasing u; it becomes purely imaginary at $u\simeq 6.0$, but shortly after it leaves the Im(ω)−axis.

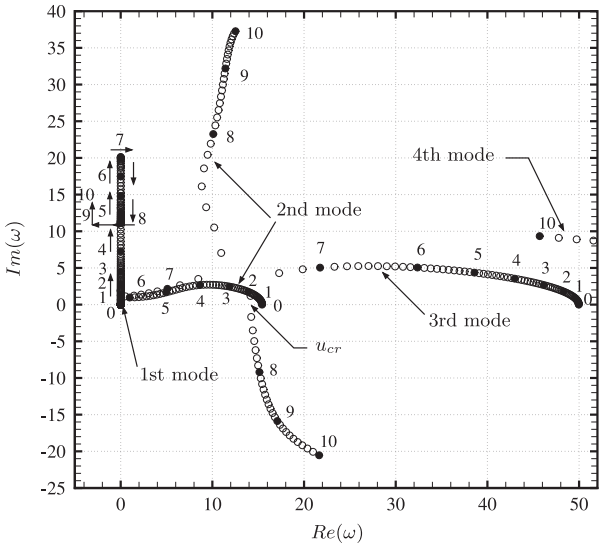

Fig. 4. The dimensionless complex frequency as a function of u for a pinned-free pipe conveying fluid and $\beta=0.2$. Arrows show the evolution of the first mode; these arrows should not be confused with the arrows used for annotation; u_{cr} represents the critical value of u for onset of instability.

Fig. 5 shows the variation of dimensionless critical flow velocity, u_{cr}, of a pinned-free pipe conveying fluid as a function of β. It is seen from this figure that, over a wide range of β ($0.15 \le \beta \le 1.0$), u_{cr} varies only gradually as β increases; for smaller β ($0 < \beta < 0.15$), however, u depends strongly on β. It is also found that there is an S-shaped segment, associated with the instability–restabilization–instability sequence (see Païdoussis, 1998, Section 3.5.1), in a narrow range of β ($0.15 \le \beta \le 0.16$).[12] Another interesting dynamical feature of a pinned-free pipe, as can be seen in this figure, is that, as $\beta \to 1$, u_{cr} does not increase without bound, contrary to a cantilevered pipe for which $u_{cr} \to \infty$, as shown by Mukhin (1965).

4.3. A pinned-free pipe conveying fluid with a rotational spring at the upstream end

Now, we turn our attention to the original problem: a pipe conveying fluid with flexible end supports. In this section, we consider a pinned-free pipe conveying fluid, additionally constrained at its upstream pinned end by a rotational spring of dimensionless stiffness κ_0^*. To come close to the pinned-free condition, we let $\kappa_0 = 10^9$ and $\kappa_1 = \kappa_1^* = 0$. Similar to previous sections, $N=40$ and 100 digits are used for the numerical calculations.

As mentioned previously, one may use an Argand diagram to present the dynamical behaviour of a pipe conveying fluid, as one of the system parameters, e.g., the flow velocity, is varied. One may also study the effect of several design parameters such as stiffness of end-supports and mass ratio (β) on the stability of the system; more specifically, on the onset of first instability. Fig. 6 shows such a study for a pinned-free system supported by an additional rotational spring κ_0^*. This figure shows variation of the onset of the first instability, u_{cr}, of the system as a function of κ_0^*, for different values of β (β = 0.2, 0.25, 0.30, 0.35 and 0.50).

The curves in Fig. 6 can be sorted into three groups. The *first* group consists of the curves associated with $\beta=0.20$ and $\beta=0.25$; for these values of the mass ratio, the system becomes less stable as κ_0^* takes on large values, whereas it is more stable as κ_0^* takes on very small values; moreover, at a specific value of κ_0^*, in the range $10^{-1} < \kappa_0^* < 10^{1}$, the system develops instability with the minimum u_{cr}; in the curves of this group, a sharp jump in u_{cr} occurs within a specific range of κ_0^*($10^{-5} \le \kappa_0^* \le 10^{-6}$). The *second* group of curves includes the curves of $\beta=0.35$ and $\beta=0.50$; it is evident from the figure that the system associated with this group of β, behaves in the opposite sense, with respect to the first group, as κ_0^* becomes very large or very small; also, in the curves of this group, the minimum u_{cr} lasts over a relatively wide range of κ_0^*, in contrast to the first group; also, there is no sharp increase in u_{cr} similar to the first group curves. The last group, the *third* group, has only one curve, $\beta=0.30$; this curve shares some features of the first group and some of the second group; it basically shows the transition from the curves of the first group to those of the second one.

The sharp jump in the curves associated with the first and third groups, in the range of $10^{-4} \le \kappa_0^* \le 10^{-6}$ (see Appendix D), can be attributed to the so-called *mode exchange* or *role reversal* characteristic. In this case, a slight change in a design parameter, such as β or κ_0^*, can make a previously unstable mode, the 2nd mode here, stable, while resulting in instability via another mode, the 3rd mode here, commonly at a different flow velocity, thus causing a sharp jump in the curve of u_{cr}. The *mode exchange* or *role reversal* is a well-known feature of the dynamics of several systems; for example, for a cantilevered pipe conveying fluid, as mentioned in Païdoussis (1998).

[12] In fact, the restabilization phase of the sequence manifests itself as a (series of) negative-slope line(s) in the segment.

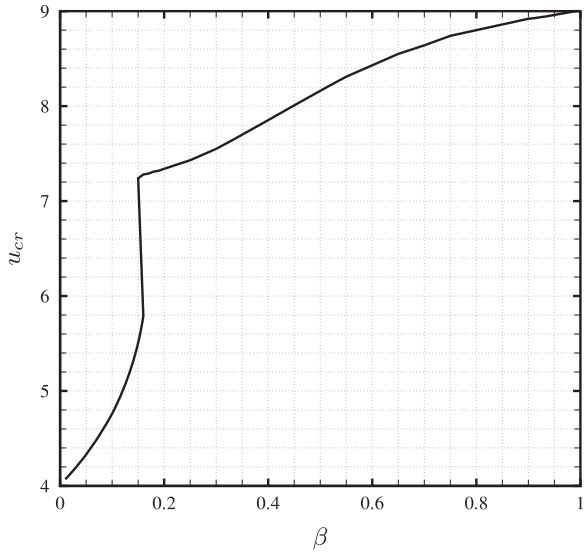

Fig. 5. The dimensionless critical flow velocity for flutter, u_{cr}, of a pinned-free pipe conveying fluid as a function of β.

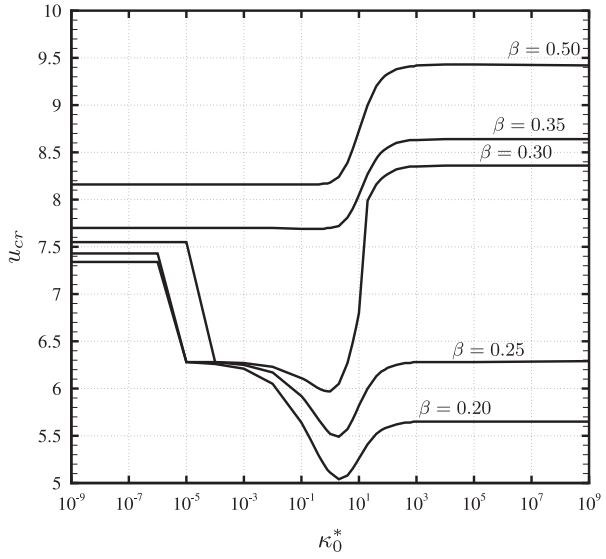

Fig. 6. Variation of u_{cr} for a pinned-free pipe conveying fluid, additionally supported at the pinned end by a rotational spring of stiffness κ_0^*, as a function of κ_0^*, for different values of β.

Fig. 6 shows that the dependence of u_{cr} on β is very strong for very high values of κ_0^*, while it is relatively weak at very low values of κ_0^*. In fact, with very large κ_0^*, the system resembles a clamped-free (cantilevered) pipe conveying fluid, for which the strong dependence of u_{cr} on β has been known for a long time (Gregory and Païdoussis, 1966a). On the other hand, as seen in the figure, vanishing values of κ_0^* have a negligible effect on the dynamics of the system, a fact that has been explained in Section 4.2 and shown in Fig. 5. This is because, for very small values of κ_0^*, the system behaves similarly to a pinned-free pipe conveying fluid.

The results shown in Fig. 6 for $\beta=0.2$ can also be compared with some results obtained by Guran and Plaut (1994a). In that paper, stability of a pinned-free pipe conveying fluid, additionally constrained at the pinned end by a rotational spring has been studied briefly. There, it was assumed that the stiffness of the spring is flow-dependent; more specifically, the nondimensional stiffness was assumed to have the form $\kappa_0^*(u)=\kappa_0^*(1+\alpha u^2)$, from which it is evident that the stiffness is constant if $\alpha=0$. Thus, the curve given in Fig. 3 of Guran and Plaut (1994a) for $\alpha=0$ can be compared with the curve for $\beta=0.2$ in Fig. 6. Although comparison is possible only for a small range of κ_0^*, $10^{-1}\le\kappa_0^*\le 10^2$, this being the range in Fig. 3 of Guran and Plaut (1994a), the two curves are in very good agreement, both qualitatively and quantitatively: the maximum relative error is $\simeq 0.9\%$. The values of u_{cr} as $\kappa_0^*\to\infty$ and $\kappa_0^*\to 0$ are found to approach $u=5.59$ and $u=6.12$, respectively, in that study. Here, as shown in Fig. 6, as κ_0^* is increased to very large values, we have $u\simeq 5.65$. As also seen in the figure, in the

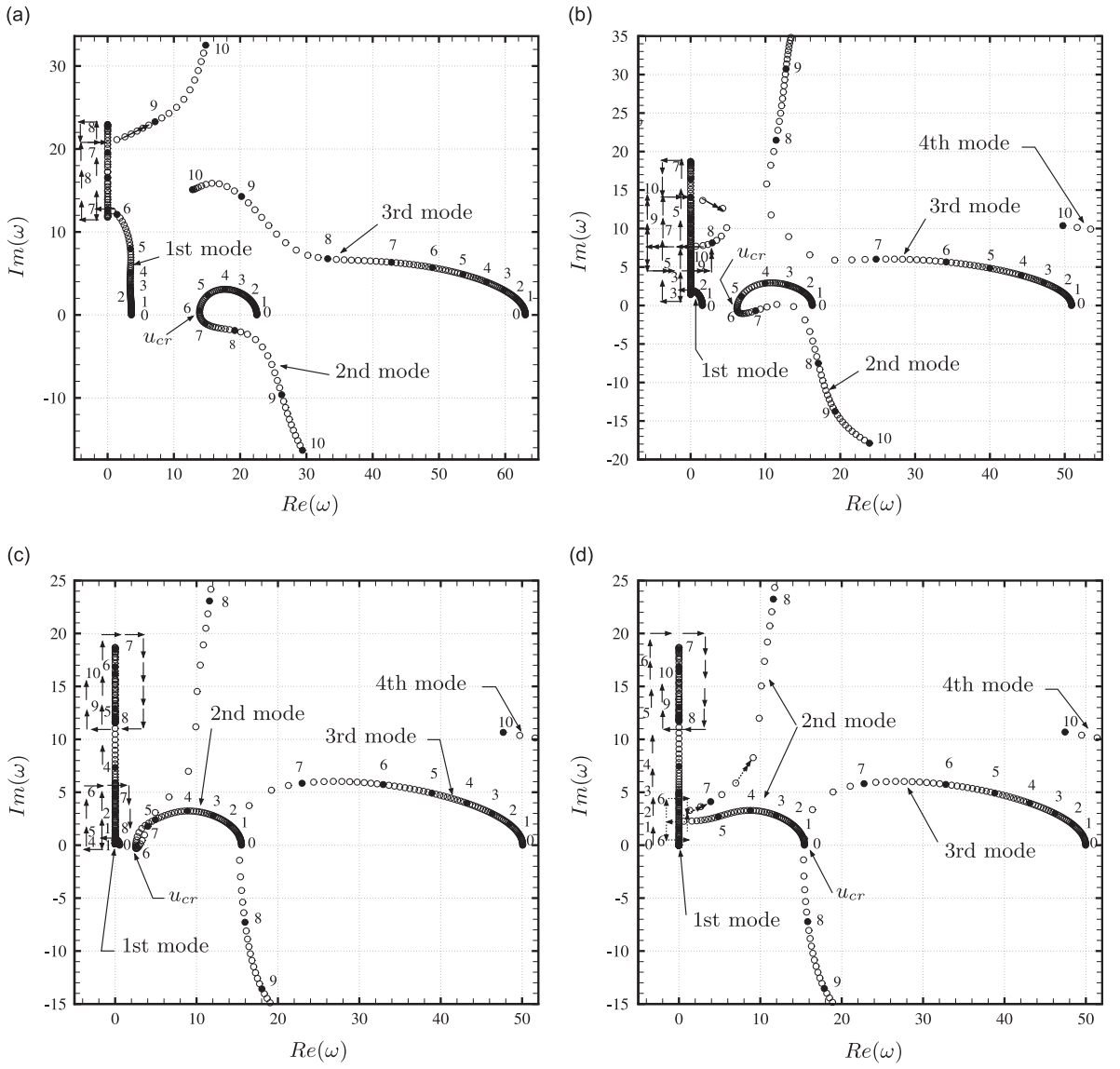

Fig. 7. Argand diagrams showing the evolution of the first three modes of a pinned-free pipe conveying fluid, further constrained by a rotational spring of stiffness κ_0^* at the pinned end, for $\beta=0.25$ and (a) $\kappa_0^*=10^8$, (b) $\kappa_0^*=10^0$, (c) $\kappa_0^*=10^{-1}$ and (d) $\kappa_0^*=10^{-8}$. Arrows with solid line show the evolution of the first mode and those with dotted line the evolution of the second mode; these arrows should not be confused with the arrows used for annotation; u_{cr} represents the critical value of u for onset of instability.

range of $10^{-5}\leq\kappa_0^*\leq10^{-4}$, u_{cr} seems to approach to a constant value of $u\simeq6.28$, again similar to that obtained by Guran and Plaut; however, at slightly lower values of κ_0^*, u undergoes a sharp jump, reaching the value of $u\simeq7.34$.

The evolution of lowest three dimensionless eigenfrequencies of the system[13] as the flow velocity u varies is given in Fig. 7(a)–(d) for $\beta=0.25$ and in Fig. 8(a)–(d) for $\beta=0.35$ for different values of κ_0^*, i.e. $\kappa_0^*=10^8,10^0,10^{-1}$ and 10^{-8} for $\beta=0.25$ and $\kappa_0^*=10^8,10^1,10^0$ and 10^{-8} for $\beta=0.35$. The numerals in the figures, close to the loci correspond to the values of u; arrows show the evolution of the first mode and in some cases also of the second mode. As seen from Fig. 7(a)–(d) and 8(a)–(d), as κ_0^* is decreased from 10^8 to 10^{-8}, the second mode gradually ceases to be the one giving rise to instability, while the third mode does the opposite. Throughout this evolution of the second and third modes, the first mode remains stable but, as κ_0^* decreases, changes from a basically flexural mode to a completely rigid-body mode, while remaining on the Im(ω)−axis. In fact, the locus of the first mode in some cases becomes very complex, and following it can be difficult; for example, in Fig. 8(c). As seen in the figure, the first mode is quickly diminished and becomes purely imaginary ($u<2$); then, it bifurcates on the Im(ω)−axis, progressing in opposite directions; at higher flow velocities ($u\simeq6.5$), the two branches

[13] The fourth mode has only partially been shown in some cases.

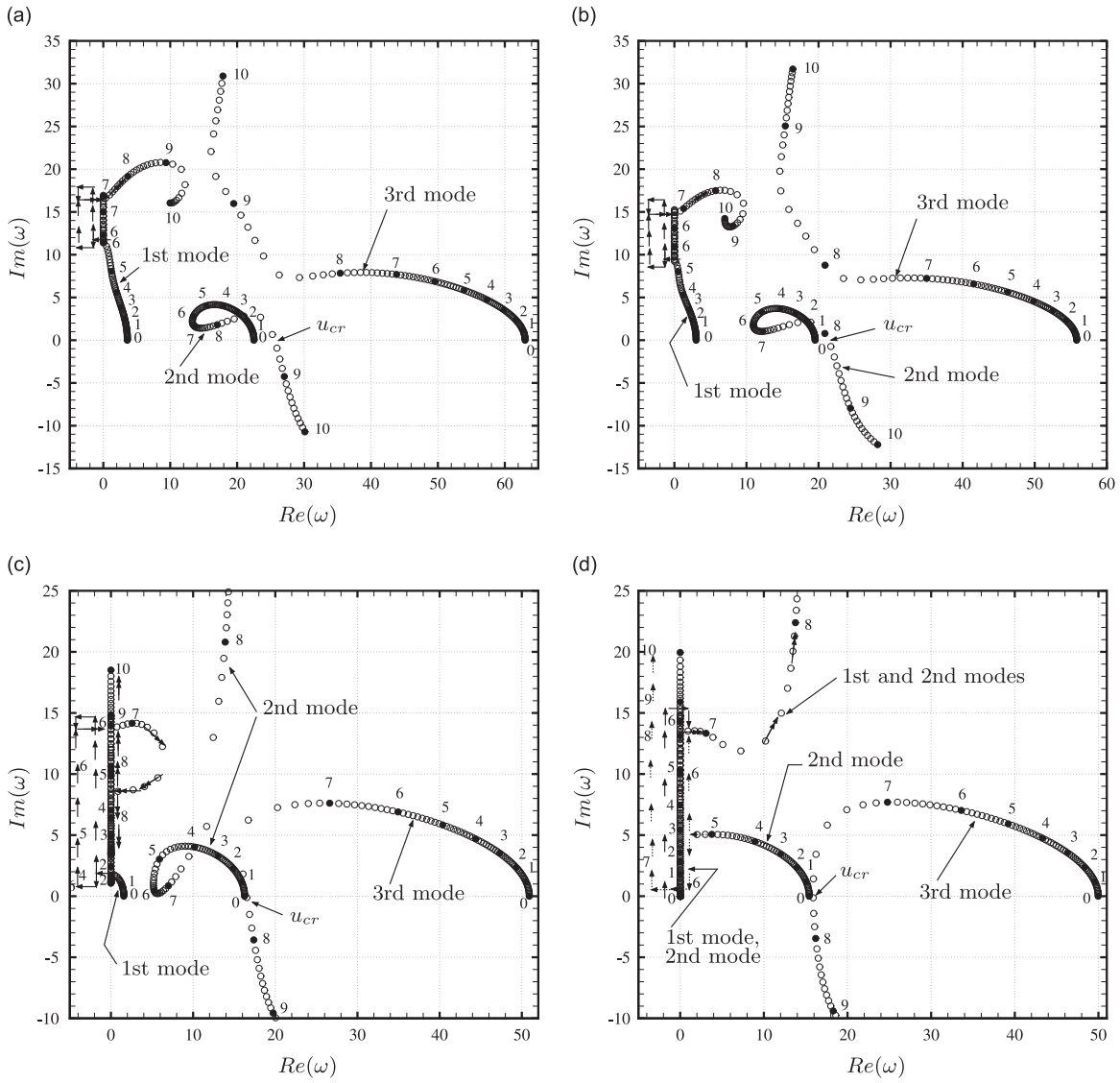

Fig. 8. Argand diagrams showing the evolution of the first three modes of a pinned-free pipe conveying fluid, further constrained by a rotational spring of stiffness κ_0^* at the pinned end, for $\beta = 0.35$ and (a) $\kappa_0^* = 10^8$, (b) $\kappa_0^* = 10^1$, (c) $\kappa_0^* = 10^0$ and (d) $\kappa_0^* = 10^{-8}$. Arrows with solid line show the evolution of the first mode and those with dotted line the evolution of the second mode; these arrows should not be confused with the arrows used for annotation; u_{cr} represents the critical value of u for onset of instability.

coalesce and leave the Im(ω)−axis, but soon after, the combined branch returns to the Im(ω)−axis and bifurcates again on the axis. The loci of the second and third modes, on the other hand, are not generally very complicated; an exception is seen in the Argand diagram of Fig. 7(d), in which the second mode eigenfrequency is gradually diminished and finally becomes purely imaginary; then, the locus bifurcates on the Im(ω)−axis, but at higher flow velocities the two branches coalesce, and the combined branch leaves the axis.

Fig. 9(a)–(h) shows the modal shape of the unstable modes of the systems whose dynamics has been presented in Figs. 7 and 8. Each sub-figure, denoted by (a)–(h), contains 16 equally spaced consecutive frames of a cycle of periodic oscillations, constructed by following the procedure presented in Kheiri et al. (2013b), at $u = 1.01u_{cr}$, where u_{cr} is the value of u for onset of instability; see Fig. 10(a,b) which is in fact the enlarged version of Fig. 9(a) and (e), respectively, and shows with the aid of numbers how the modal shape develops with time during a cycle of periodic oscillations. As seen in Fig. 9(a)–(h), in almost all of the sub-figures, a strong traveling-wave component is present, showing that the normal modes are non-classical (Païdoussis, 1998). It is also evident from Fig. 9(a)–(c) that the flexure present in the unstable mode, the second mode, is gradually diminished, and the initial flexural mode shape finally becomes quasi-rigid. Comparison between Fig. 9(a) and (e) and between Fig. 9(d) and (h) also indicates that the shape of the unstable mode is strongly dependent on β for $\kappa_0^* = 10^8$, while it is weakly dependent on β for $\kappa_0^* = 10^{-8}$. A similar conclusion was previously reached in connection with the

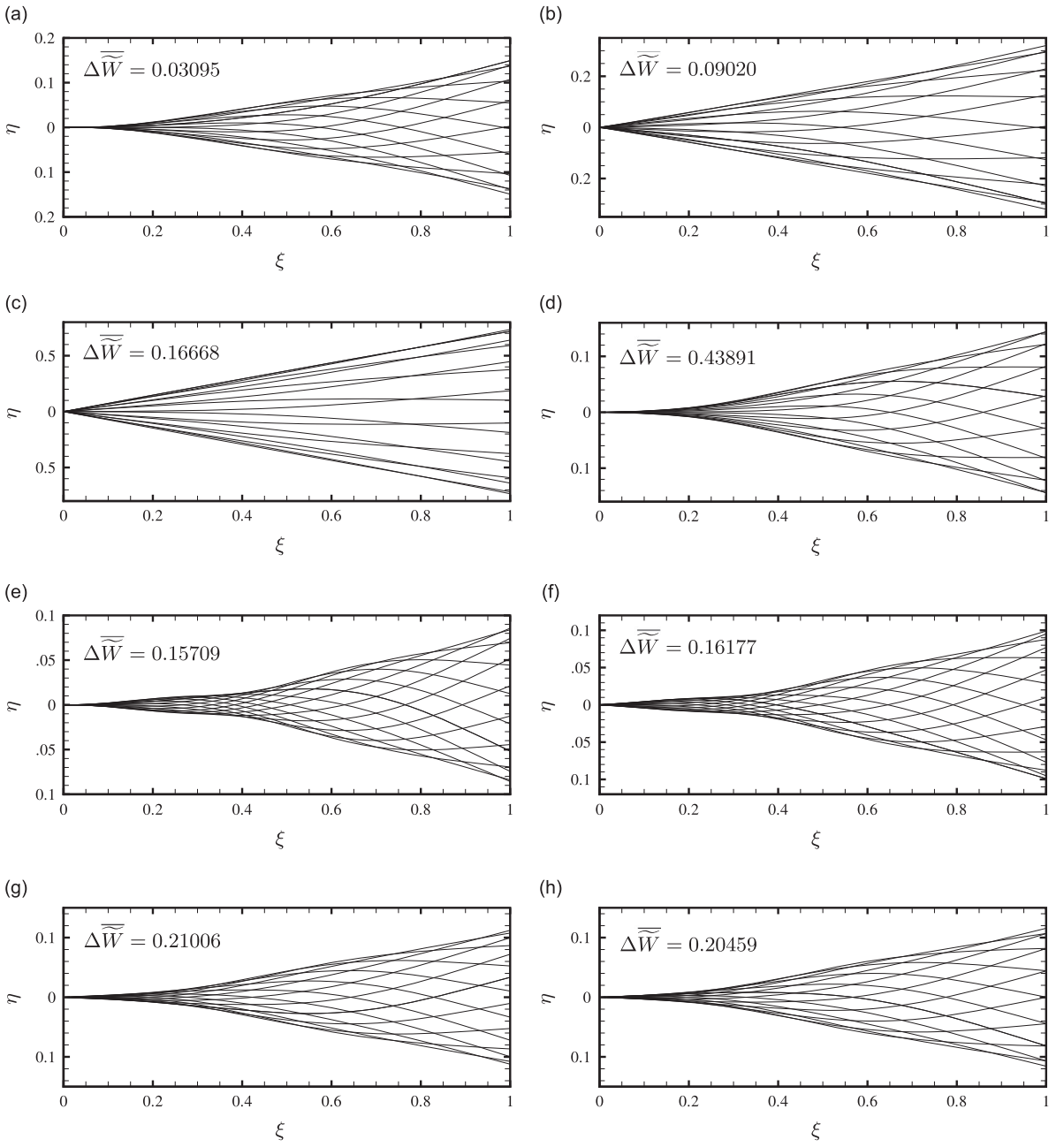

Fig. 9. Modal shapes of the unstable modes of a pinned-free pipe conveying fluid, further constrained by a rotational spring of stiffness κ_0^* at the pinned end: (a, e): $\kappa_0^* = 10^8$, (b, g): $\kappa_0^* = 10^0$, (c): $\kappa_0^* = 10^{-1}$, (d, h): $\kappa_0^* = 10^{-8}$ and (f): $\kappa_0^* = 10^1$; for (a–d): β=0.25 and for (e–h): β=0.35. Each figure shows 16 consecutive, equally spaced frames in a cycle of oscillation; they have been constructed at $u \simeq 1.01 u_{cr}$, where u_{cr} is: (a) 6.28, (b) 5.52, (c) 5.92, (d) 7.43, (e) 8.64, (f) 8.05, (g) 7.70 and (h) 7.70. In the figures, $\Delta\widetilde{\overline{W}}$ gives the time-averaged dimensionless energy transfer from the flow to the pipe.

dependence of u_{cr} on β, shown in Fig. 6. This seems reasonable, because it indicates that the pipe assumes a different shape to be able to absorb more/less energy from the flow, and so becomes unstable earlier/later.

The energy transfer from the fluid to the pipe can also be calculated for each mode shape shown in Fig. 9(a)–(e) to verify the occurrence of instability in the system, with the specific mode involved. Thus, Eq. (28) is used to obtain the time-averaged dimensionless energy transfer, $\Delta\widetilde{\overline{W}}$, from flow to the pipe; they are given in the top left part of each sub-figure. As seen, $\Delta\widetilde{\overline{W}}$ is positive for all mode shapes shown in Fig. 9(a)–(e), confirming the occurrence of the instability in that mode shape. It is noted that to obtain reasonably accurate results, the cycle of oscillation is divided into at least 256 equally spaced instants, and all quantities are averaged out over such a cycle.

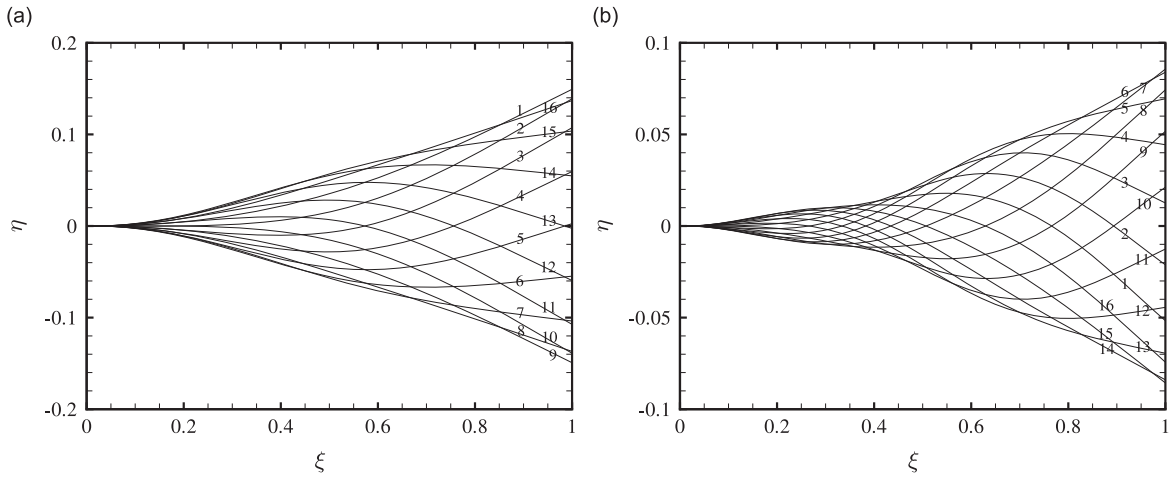

Fig. 10. Redrawing of the modal shapes shown in Fig. 9(a) and (e), in (a) and (b), respectively. In this figure, the numbers 1–16 represent the sequence of deformed shapes for one cycle of periodic oscillations.

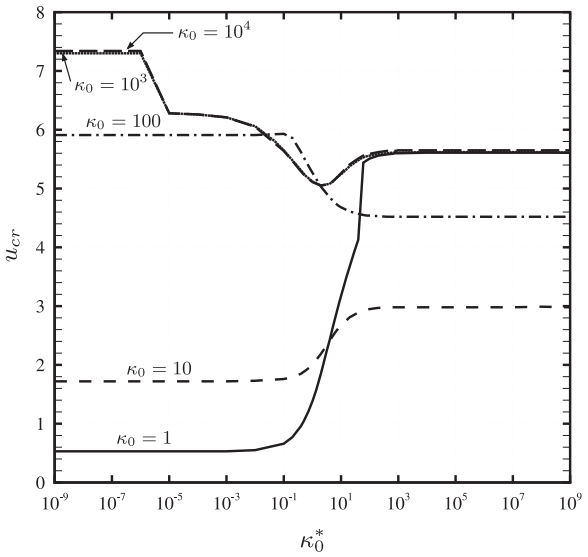

Fig. 11. Variation of u_{cr} for a pipe conveying fluid supported by a translational spring of stiffness κ_0 and a rotational spring of stiffness κ_0^* at the upstream end and free at the other, as a function of κ_0^*, at different values of κ_0.

4.4. A pipe conveying fluid supported only by a translational and a rotational spring at the upstream end

This section is devoted to the study of dynamics of a pipe conveying fluid supported by a translational and a rotational spring of dimensionless stiffnesses κ_0 and κ_0^*, respectively, at the upstream end and free at the other. First, consider Fig. 11 which shows the variation of the critical flow velocity of the system, u_{cr}, as a function of κ_0^* for several values of κ_0, i.e. $\kappa_0 = 1, 10, 100, 10^3$ and 10^4. The major dynamical feature of this system, as seen in the figure, is that the system may display a wide variety of behaviour, which in fact is not easily predictable, especially for lower values of κ_0, as κ_0 and κ_0^* vary. For example, one can notice that u_{cr} varies with κ_0^* in a very different way in the two cases of $\kappa_0 = 10$ and $\kappa_0 = 100$; the former generally shows an increasing trend, while the latter displays the opposite trend, as κ_0^* is increased. In the case of $\kappa_0 = 1$, the corresponding curve follows a similar trend to the curve for $\kappa_0 = 10$, but with lower values of u_{cr} in the range of $\kappa_0^* < 4$, and outside of this range it unexpectedly increases to values even higher than those associated with $\kappa_0 = 100$. In contrast to the cases with $\kappa_0 = 1, 10$ and 100 at higher values of κ_0 ($\kappa_0 = 10^3$ and 10^4), as κ_0^* increases, the critical flow velocity first experiences a decrease, but it slightly increases afterwards. This type of behaviour has also been observed in Fig. 6.

The dynamics of the system is analyzed more closely for the cases where $\kappa_0^* = 1$ and $\kappa_0^* = 100$ and when $\kappa_0 = 1, 10, 100$ and 10^3, by examining the evolution of the first four eigenfrequencies of the system in the Argand diagrams. These are shown, respectively, in Figs. 12(a)–(d) and 13(a)–(d). In these figures, the arrows show the evolution of the first mode and in some cases that of the second mode also; the numerals close to the loci are the values of dimensionless flow velocities. In the first group of diagrams (Fig. 12), the first mode bifurcates on the Im(ω)−axis at relatively low flow velocities; the two

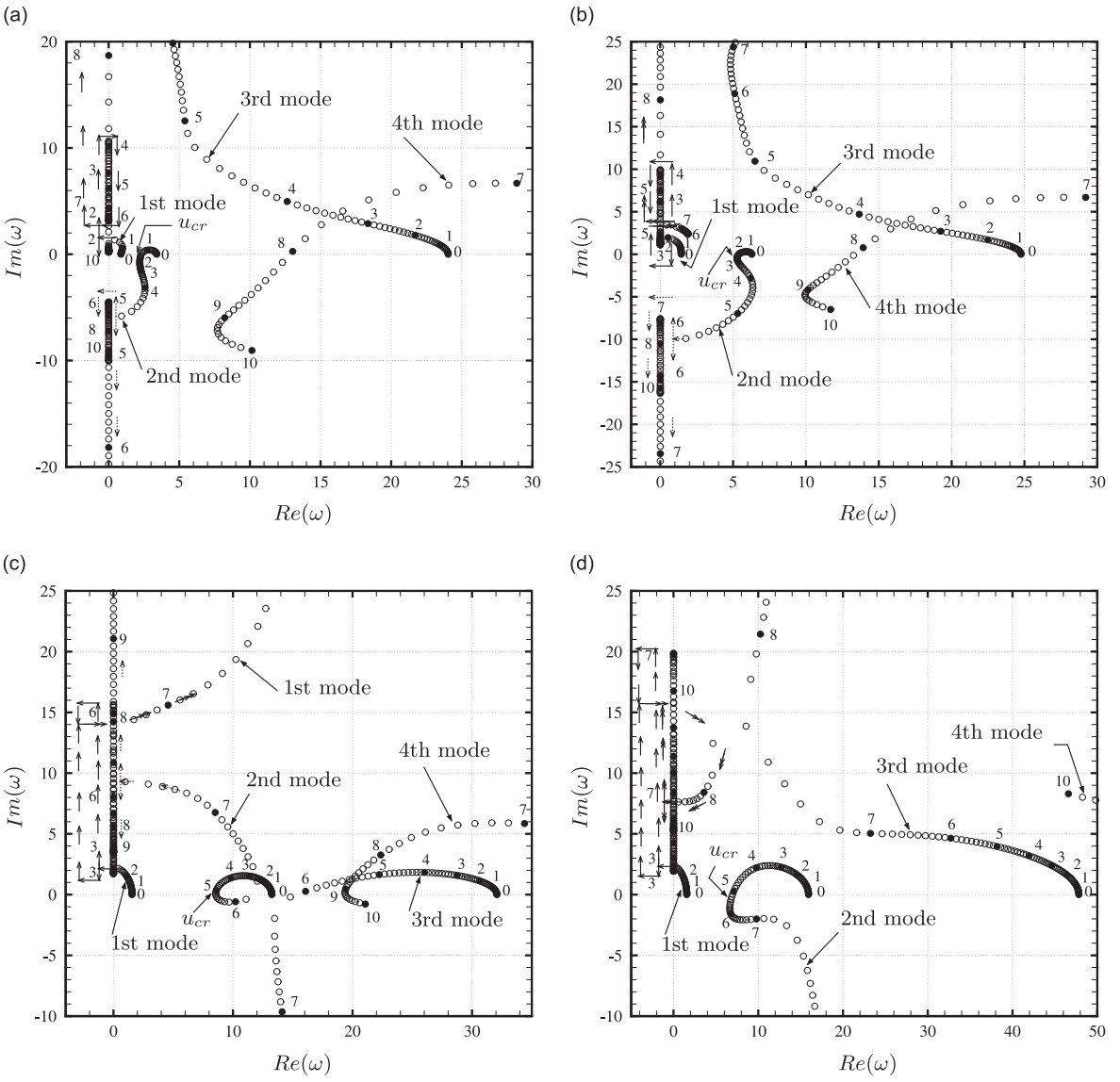

Fig. 12. Argand diagrams showing the evolution of the first four modes of a pipe conveying fluid constrained by a translational and a rotational spring of stiffnesses κ_0 and κ_0^*, respectively, at the upstream end and free at the other, for $\beta = 0.20$ and $\kappa_0^* = 1$ and for (a) $\kappa_0 = 1$, (b) $\kappa_0 = 10$, (c) $\kappa_0 = 100$ and (d) $\kappa_0 = 10^3$. Arrows with solid line show the evolution of the first mode and those with dotted line the evolution of the second mode; these arrows should not be confused with the arrows used for annotation; u_{cr} represents the critical value of u for onset of instability.

resultant branches grow with different rates, partly in opposite directions; at higher u, the two branches may coalesce and leave the Im(ω)−axis, as seen in Fig. 12(b)–(d). This mode remains stable up to the maximum flow velocity considered in the calculations, $u_{\max} = 10$. The second mode, on the other hand, develops an instability at low values of u, respectively at $u_{cr} \simeq 1.38$ and $u_{cr} \simeq 2.00$ in Fig. 12(a) and (b), and at higher values of u, respectively at $u_{cr} \simeq 5.27$ and $u_{cr} \simeq 5.12$ in 12(c) and (d). It is also interesting to see that in some cases the locus associated with the second mode becomes purely imaginary after the instability, at higher u. Except for the case shown in Fig. 12(c), the third mode is stable up to $u_{\max}$. The fourth mode also displays greater stability as κ_0 is increased.

In the second group of Argand diagrams (Fig. 13), the first mode behaves relatively similarly to what was seen in the first group of diagrams. The first instability also occurs in the second mode by flutter, via a Hopf bifurcation at, respectively, $u_{cr} \simeq 5.51$, $u_{cr} \simeq 2.95$, $u_{cr} \simeq 4.54$ and $u_{cr} \simeq 5.56$, corresponding to Fig. 13(a)-(d), respectively. As seen in the figures, the third and fourth modes are stable up to $u_{\max}$.

In Fig. 14(a)–(h), the modal shapes are shown for the unstable modes of the system presented in Figs. 12 and 13. Each modal shape is constructed at $u = 1.01u_{cr}$, where u_{cr} is the corresponding threshold of instability, and it consists of 16 equally spaced consecutive frames of a cycle of periodic oscillations. Similar to Fig. 10 in Section 4.3, enlarged versions of Fig. 14(a) and (e) are shown in Fig. 15(a) and (b), in which the numbers 1–16 on the curves show how the modal shape

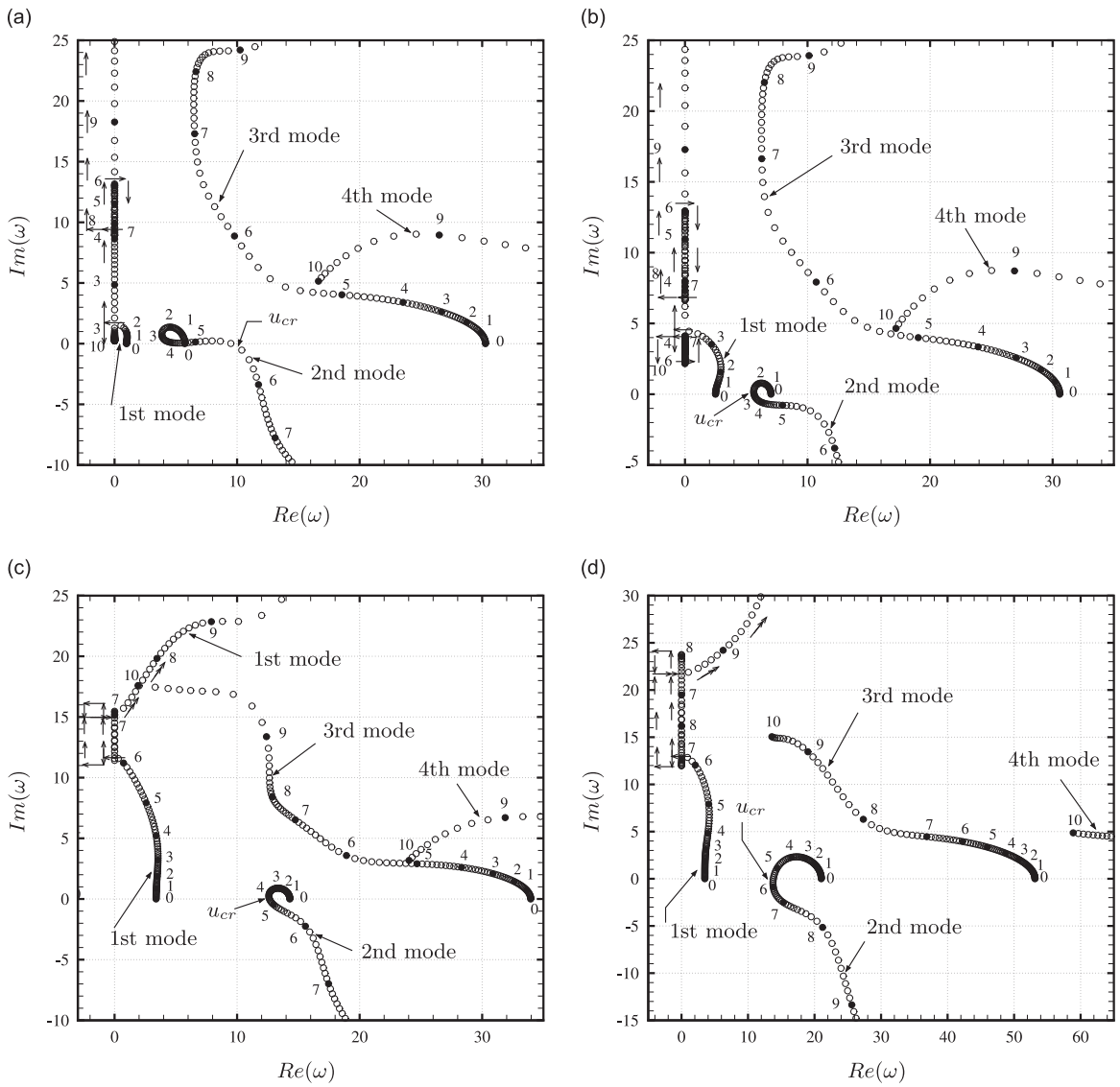

Fig. 13. Argand diagrams showing the evolution of the first four modes of a pipe conveying fluid constrained by a translational and a rotational spring of stiffnesses κ_0 and κ_0^*, respectively, at the upstream end and free at the other, for $\beta = 0.20$ and $\kappa_0^* = 100$ and for (a) $\kappa_0 = 1$, (b) $\kappa_0 = 10$, (c) $\kappa_0 = 100$ and (d) $\kappa_0 = 10^3$. Arrows show the evolution of the first mode; these arrows should not be confused with the arrows used for annotation; u_{cr} represents the critical value of u for onset of instability.

evolves during a period of oscillations. Similar to Fig. 9, there exists a strong traveling-wave component in the modal shapes presented in Fig. 14. Since the upstream end of the pipe in the present case is not rigidly fixed, contrary to the cases with classical boundary conditions, the pipe is subjected to relatively high-amplitude oscillations also at the upstream end (except for Fig. 14(d) and(h)). Furthermore, it is very interesting to see, particularly in Fig. 14(a) and (b), a type of quasi-rigid-body oscillation, very similar to the so-called *criss-crossing* oscillation[14] usually observed in the dynamics of towed systems (see, e.g., Kheiri et al., 2013a). The values of $\Delta\tilde{W}$ are also given in the figures for each unstable mode. The positive value of $\Delta\tilde{W}$ confirms that the pipe gains energy from flow, and so develops oscillatory motions.

5. Conclusion

In this paper, a general linear theoretical model has been developed for dynamics of a pipe conveying fluid flexibly restrained at both ends, allowing us to conveniently study the dynamics of pipes with both classical and non-classical boundary conditions. The equation of motion was derived via Hamilton's principle for open systems, and the effect of

[14] A rigid-body oscillation during which the two extreme positions of the body in a cycle of oscillation form an X.

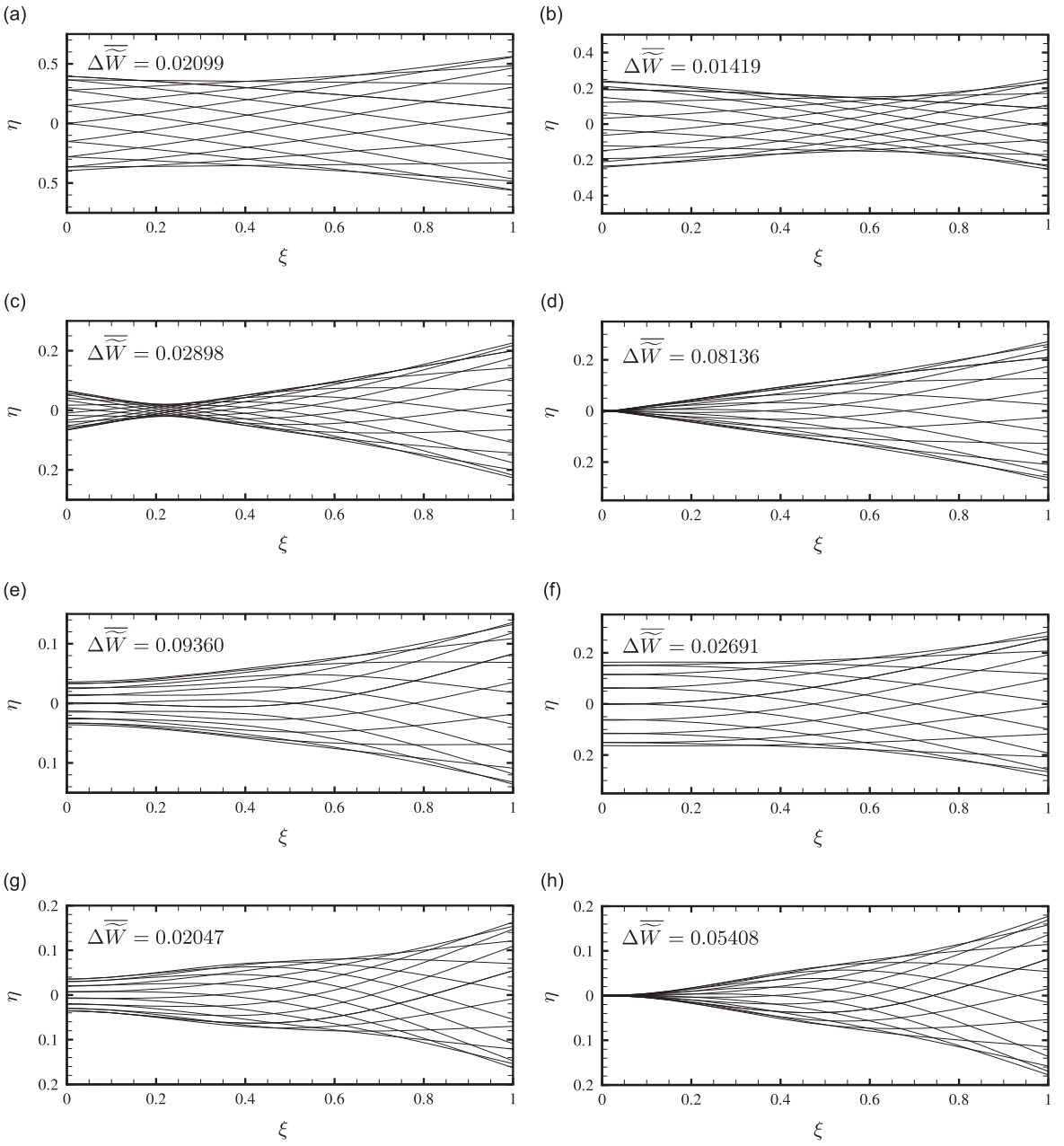

Fig. 14. Modal shapes of the unstable modes of a pipe conveying fluid constrained by a translational and a rotational spring of stiffnesses κ_0 and κ_0^*, respectively, at the upstream end and free at the other: (a, e): $\kappa_0 = 1$, (b, f): $\kappa_0 = 10$, (c, g): $\kappa_0 = 100$ and (d, h): $\kappa_0 = 10^3$; for (a–d): $\kappa_0^* = 1$ and for (e–h): $\kappa_0^* = 100$. Each figure shows 16 consecutive, equally spaced frames in a cycle of oscillation; they have been constructed at $u \simeq 1.01u_{cr}$, where u_{cr} is: (a) 1.38, (b) 2.00, (c) 5.27, (d) 5.12, (e) 5.51, (f) 2.95, (g) 4.54 and (h) 5.56. In the figures, $\Delta\widetilde{\widetilde{W}}$ gives the time-averaged dimensionless energy transfer from the flow to the pipe.

flexible end-supports was systematically incorporated in the equation of motion, rather than in the boundary conditions. The dimensionless form of the equation of motion was then discretized via Galerkin's method in which the eigenfunctions of a free–free Euler–Bernoulli beam were utilized as comparison functions. The resulting set of second-order ODEs was then used to perform various analyses.

For a beam flexibly supported at the ends, the eigenvalues of free vibration were obtained numerically for three different cases, where they were found to be in very good agreement with existing numerical results. The dynamics of a pinned-free pipe conveying fluid was then investigated in some detail; it was found that a pinned-free pipe conveying fluid is *neutrally* stable at low flow velocities; however, at sufficiently high flow velocities it becomes subject to instability, generally in the form of a single-mode flutter. It was also found that for a small range of mass ratio ($0 < \beta \leq 0.16$), the onset of instability

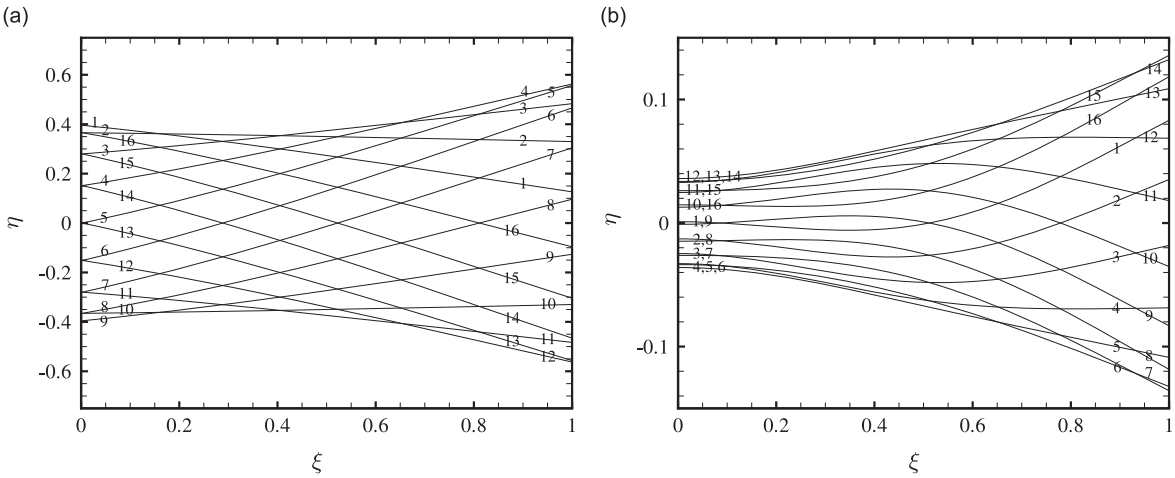

Fig. 15. Redrawing of the modal shapes shown in Fig. 14(a) and (e), in (a) and (b), respectively. In this figure, the numbers 1–16 represent the sequence of deformed shapes for one cycle of periodic oscillations.

increases sharply as β increases, while for the rest of the range it changes only gradually with β. Moreover, in a very narrow range of β, the system undergoes the instability–restabilization–instability sequence, a feature which has previously been observed in the dynamics of, for example, a cantilevered pipe conveying fluid.

The next system whose dynamics was studied in detail, is a pinned-free pipe conveying fluid additionally constrained by a variable rotational spring at the pinned end. It was shown that the onset of instability, flutter, at moderate to large values of spring stiffness strongly depends on the mass ratio, whereas it is weakly dependent on β at low values of stiffness. It was also found that, depending on β, there is a range of spring stiffness within which an increase in the stiffness renders the pipe *less* stable. Also, for low values of β, a relatively sharp jump in the values of the critical flow velocity may emerge, as a result of a mode exchange or role reversal phenomenon. Except for these jumps, the critical flow velocity was found to be insensitive to the spring stiffness at sufficiently high or low values of the stiffness.

Finally, a pipe conveying fluid constrained only by a translational and a rotational spring at the upstream end was considered. It was found that making the springs, one or both of them, stiffer will not necessarily have a stabilizing effect on the system. It was also found that there are ranges of stiffness in which the critical flow velocity does not change with changing either of the stiffnesses. It was also shown that, as the stiffnesses are reduced to low values, the system approaches that of a free-free pipe: the critical flow velocity is diminished and finally approaches zero. In the modal shapes of the unstable modes of this system, contrary to pipes with classical boundary conditions, both upstream and downstream ends may undergo displacements, resembling quasi-rigid-body modes of flexible cylindrical systems subjected to external axial flow.

It should be stressed that the authors are fully aware of the limitations of linear theory, the theory used in the present paper. However, linear theory ought to be used first, before any attempt is made to analyze the system by a more realistic nonlinear theory. This first analysis is presented in this paper. Moreover, as is well known, linear theory ceases giving reliable predictions once the threshold of the first instability is exceeded; for that reason, emphasis has been placed in this paper on the "first instability". The threshold for that first instability is reliable, so long as the bifurcation involved is supercritical, which, as shown in Païdoussis (1998), is most often the case. Nevertheless, it is clear that all of the results reported in this paper need to eventually be validated by nonlinear theory, not a trivial task, but one that nonetheless will soon be undertaken.

Acknowledgments

The support to this research by the Natural Sciences and Engineering Research Council of Canada (NSERC) and Solution Mining Research Institute (SMRI) is gratefully acknowledged. The first author is also grateful to the Faculty of Engineering of McGill University for a McGill Engineering Doctoral Award (MEDA) to assist in his Ph.D. studies.

Appendix A. The expressions for the forces exerted on the funnel (system1)

Consider Fig. A1 in which a control volume containing system1 (the funnel, the coupling and the fluid within) is shown. As seen in the figure, flow enters the control volume through an area of A_i with a velocity of $v\boldsymbol{i}$, and leaves it with a velocity of $U\boldsymbol{\tau}|_{x=0}$ through an area of A (the same as the cross-sectional area of the pipe); the hydrostatic pressure at the inlet (over most of the inlet) is $p_i^{(1)}$ and that at the exit is $p_e^{(1)}$. It is noted that $p_i^{(1)}$ and $p_e^{(1)}$ are measured above the atmospheric pressure; this is because the net force due to the uniform atmospheric pressure acting on the control volume is zero, according to the *divergence* or *Gauss's* theorem.

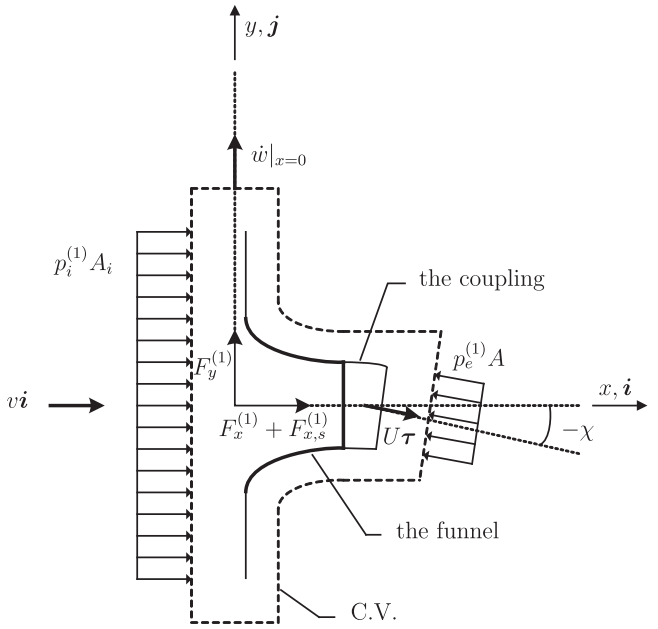

Fig. A1. The control volume containing the funnel, the coupling and the fluid inside them; $v\boldsymbol{i}$ is the mean upstream flow velocity and $U\boldsymbol{\tau}$ is the fluid velocity inside the pipe; flow enters the control volume through an area of A_i, on which a static pressure $p_i^{(1)}$ acts, and it leaves it through an area of A, where the static pressure is $p_e^{(1)}$. The control volume moves with velocity $\dot{w}|_{x=0}$ in the y-direction.

Now, let us write the linear momentum equation for the control volume shown in Fig. A1:

$$\sum \boldsymbol{F}_{\text{sys}} = \frac{d}{dt}\iiint_{V_1} \rho \boldsymbol{u}\, \mathrm{d}V + \iint_{S_i^{(1)}, S_e^{(1)}} \rho \boldsymbol{u}(\boldsymbol{u}-\boldsymbol{V})\cdot \boldsymbol{n}\, \mathrm{d}S, \tag{A.1}$$

in which $\sum \boldsymbol{F}_{\text{sys}}$ is the vector sum of all external forces acting on the system; $\boldsymbol{u}$ is the fluid velocity and $\boldsymbol{V}$ is the velocity of the control surface; $\boldsymbol{n}$ is the outward normal unit vector on the control surface.

Eq. (A.1) may then be expanded as

$$F_x^{(1)}\boldsymbol{i} + F_y^{(1)}\boldsymbol{j} + F_{x,s}^{(1)}\boldsymbol{i} + p_i^{(1)}A_i\boldsymbol{i} - p_e^{(1)}A\boldsymbol{\tau}|_{x=0} = \iint_{S_i^{(1)}} (v\boldsymbol{i})\rho(v\boldsymbol{i} - \dot{w}|_{x=0}\boldsymbol{j})\cdot(-\boldsymbol{i})\, \mathrm{d}S + \iint_{S_e^{(1)}} [(U\boldsymbol{\tau} + \dot{w}\boldsymbol{j})\rho(U\boldsymbol{\tau})\cdot\boldsymbol{\tau}]_{x=0}\, \mathrm{d}S, \tag{A.2}$$

where $F_x^{(1)}$ and $F_y^{(1)}$ are the forces, respectively, in the x- and y-directions, which are exerted on system1 by system2; $F_{x,s}$ is the force, in the x-direction, due to the presence of the supports. Also, to obtain the above equation, the inertial forces due to the fluid mass contained in the control volume has been neglected as the size of the funnel is assumed to be very small.

$F_x^{(1)}$ and $F_y^{(1)}$ may finally be found after performing some manipulations on Eq. (A.2):

$$\begin{aligned} F_x^{(1)} &= -F_{x,s}^{(1)} + p_e^{(1)}A\, \cos\chi|_{x=0} - p_i^{(1)}A_i^{(1)} + \rho A U^2\, \cos\chi|_{x=0} - \rho A_i^{(1)} v^2, \\ F_y^{(1)} &= p_e^{(1)}A\, \sin\chi|_{x=0} + \rho A U^2\, \sin\chi|_{x=0} + \rho A U \dot{w}|_{x=0}. \end{aligned} \tag{A.3}$$

Therefore, $F_x^{(2)}$ and $F_y^{(2)}$ which are the reactions of $F_x^{(1)}$ and $F_y^{(1)}$, respectively, may simply be written as

$$\begin{aligned} F_x^{(2)} &= -[-F_{x,s}^{(1)} + p_e^{(1)}A\, \cos\chi|_{x=0} - p_i^{(1)}A_i^{(1)} + \rho A U^2\, \cos\chi|_{x=0} - \rho A_i^{(1)} v^2], \\ F_y^{(2)} &= -[p_e^{(1)}A\, \sin\chi|_{x=0} + \rho A U^2\, \sin\chi|_{x=0} + \rho A U \dot{w}|_{x=0}]. \end{aligned} \tag{A.4}$$

Appendix B. Some elaboration on the derivation of the equation of motion and boundary conditions

Let us restart with Eq. (11) along with considering $\overline{\kappa} \simeq w'' + O(\epsilon^2)$ (in the linear form); $\delta \int_{t_1}^{t2} \mathcal{V}\, \mathrm{d}t$ can then be written as

$$\delta \int_{t_1}^{t_2} \mathcal{V}\, \mathrm{d}t = \int_{t_1}^{t_2}\int_0^L EIw''\delta w''\, \mathrm{d}s\, \mathrm{d}t + \int_{t_1}^{t_2} [K_0 w_0 \delta w_0 + C_0 w_0' \delta w_0' + K_L w_L \delta w_L + C_L w_L' \delta w_L']\, \mathrm{d}t. \tag{B.1}$$

Using integration by parts, the first right-hand integral can be expanded as

$$\int_0^L EIw''\delta w''\, \mathrm{d}s = EIw''\delta w'|_0^L - EIw'''\delta w|_0^L + \int_0^L EIw''''\delta w\, \mathrm{d}s. \tag{B.2}$$

By substituting Eq. (B.2) into (B.1), one can obtain

$$\delta\int_{t_1}^{t_2}\mathcal{V}\,\mathrm{d}t=\int_{t_1}^{t_2}\int_0^L EIw''''\delta w\,\mathrm{d}s\,\mathrm{d}t+\int_{t_1}^{t_2}[EIw''\delta w'-EIw'''\delta w]_0^L\,\mathrm{d}t + \int_{t_1}^{t_2}[K_0w_0\delta w_0+C_0w_0'\delta w_0'+K_Lw_L\delta w_L+C_Lw_L'\delta w_L']\,\mathrm{d}t. \tag{B.3}$$

Now, from Eqs. (8), (10) and (B.3) one can express $\delta\int_{t_1}^{t_2}\mathcal{L}_o\mathrm{d}t+\int_{t_1}^{t_2}\delta\mathcal{H}\,\mathrm{d}t$ as

$$\begin{aligned}\delta\int_{t_1}^{t_2}\mathcal{L}_o\,\mathrm{d}t+\int_{t_1}^{t_2}\delta\mathcal{H}\,\mathrm{d}t=&-\int_{t_1}^{t_2}\int_0^L[(m+M)\ddot{x}+2MU\dot{x}']\delta x\,\mathrm{d}s\,\mathrm{d}t\\&-\int_{t_1}^{t_2}\int_0^L[(m+M)\ddot{w}+2MU\dot{w}']\delta w\,\mathrm{d}s\,\mathrm{d}t\\&+MU\int_{t_1}^{t_2}[\dot{x}_L\delta x_L+\dot{w}_L\delta w_L]\,\mathrm{d}t-MU\int_{t_1}^{t_2}[\dot{x}_0\delta x_0+\dot{w}_0\delta w_0]\,\mathrm{d}t\\&-\int_{t_1}^{t_2}\int_0^L EIw''''\delta w\,\mathrm{d}s\,\mathrm{d}t-\int_{t_1}^{t_2}[EIw''\delta w'-EIw'''\delta w]_0^L\,\mathrm{d}t\\&-\int_{t_1}^{t_2}[K_0w_0\delta w_0+C_0w_0'\delta w_0'+K_Lw_L\delta w_L+C_Lw_L'\delta w_L']\,\mathrm{d}t+\int_{t_1}^{t_2}\delta\overline{\mathcal{W}}\,\mathrm{d}t\\&-MU^2\int_{t_1}^{t_2}[x_L'\delta x_L+w_L'\delta w_L]\,\mathrm{d}t-MU\int_{t_1}^{t_2}[\dot{x}_L\delta x_L+\dot{w}_L\delta w_L]\,\mathrm{d}t.\end{aligned} \tag{B.4}$$

Since there are no other external forces acting on the system, $\int_{t_1}^{t_2}\delta\overline{\mathcal{W}}\mathrm{d}t=0$. Using Eq. (14) and neglecting terms of higher order than ϵ, Eq. (B.4) reduces to

$$\begin{aligned}&\delta\int_{t_1}^{t_2}\mathcal{L}_o\,\mathrm{d}t+\int_{t_1}^{t_2}\delta\mathcal{H}\,\mathrm{d}t\\&\quad=-\int_{t_1}^{t_2}\int_0^L[EIw''''+MU^2w''+2MU\dot{w}'+(m+M)\ddot{w}]\delta w\,\mathrm{d}s\,\mathrm{d}t\\&\qquad-\int_{t_1}^{t_2}[EIw''\delta w'-EIw'''\delta w]_0^L\,\mathrm{d}t-MU\int_{t_1}^{t_2}[\dot{w}_0+Uw_0']\delta w_0\,\mathrm{d}t\\&\qquad-\int_{t_1}^{t_2}[K_0w_0\delta w_0+C_0w_0'\delta w_0'+K_Lw_L\delta w_L+C_Lw_L'\delta w_L']\,\mathrm{d}t,\end{aligned} \tag{B.5}$$

where the last three integrands on the right-hand side would basically form the boundary conditions of the original system (i.e., the system shown in Fig. 1(b); they are

$$(EIw''-C_0w')\delta w'=0,\quad (EIw'''+K_0w+MU\dot{w}+MU^2w')\delta w=0\ \text{ at } s=0, \tag{B.6.1}$$

$$(EIw''+C_Lw')\delta w'=0,\quad (EIw'''-K_Lw)\delta w=0\ \text{ at } s=L, \tag{B.6.2}$$

in which since $\delta w'|_{s=0,L}$ and $\delta w|_{s=0,L}$ are generally non-zero for the original system, the terms in parentheses should vanish; therefore, they are the boundary conditions.

However, instead of dealing with non-homogenous, non-classical boundary conditions resulting from (B.6.1) and (B.6.2), which may make the solution of the problem more difficult, it is assumed that the system has the boundary conditions of a free–free beam, i.e. $EIw''=EIw'''=0$, at $s=0, L$ (see Eq. (16)). Thus, the second right-hand integral in Eq. (B.5) vanishes, while the third and fourth integrals remain in the equation and become part of the equation of motion via the use of appropriate Dirac delta functions; in fact, the presence of these terms in the equation of motion confirms that the effect of the end-springs and momentum transport into the system is considered in the formulation, although it has disappeared from the boundary conditions. As a result, by letting $[\,]\delta w_0=\int_0^L[\,]\delta w\overline{\delta}(s)\,\mathrm{d}s$ and $[\,]\delta w_L=\int_0^L[\,]\delta w\overline{\delta}(s-L)\,\mathrm{d}s$ in Eq. (B.5), where $\overline{\delta}(s)$ is the Dirac delta function, and similarly for $\delta w'$, Eq. (B.5) becomes the same as Eq. (15).

Appendix C. Analytical evaluation of b_{ij} and c_{ij}

The method to analytically evaluate b_{ij} and c_{ij} for a free-free Euler–Bernoulli beam is briefly explained here. More details on the procedure used here can be found in Appendix B of Païdoussis (1998).

First, let us treat b_{ij} when $(i,j\geq 3)$. We can re-write b_{ij} as

$$b_{ij}=\int_0^1\phi_i\phi_j'\,\mathrm{d}\xi=\frac{1}{\lambda_j^4}\int_0^1\phi_i\phi_j''''\,\mathrm{d}\xi, \tag{C.1}$$

the last term of which, after successive integration by parts, gives

$$b_{ij}=\frac{1}{\lambda_j^4}\left\{[\phi_i\phi_j''''-\phi_i'\phi_j'''+\phi_i''\phi_j''-\phi_i'''\phi_j']_0^1+\int_0^1\phi_i''''\phi_j'\,\mathrm{d}\xi\right\},\tag{C.2}$$

in which the last integral may be written as $\int_0^1\lambda_i^4\phi_i\phi_j'\,\mathrm{d}\xi=\lambda_i^4 b_{ij}$; taking this, along with applying the boundary conditions, i.e. $\phi''(0)=\phi''(1)=\phi'''(0)=\phi'''(1)=0$, as well as $\phi_i(0)=2$ and $\phi_i(1)=2(-1)^{i-3}$, and similarly for ϕ_j, yields

$$b_{ij}=\frac{4[(-1)^{i+j-6}-1]}{1-(\lambda_i/\lambda_j)^4}\quad(i,j\geq 3).\tag{C.3}$$

The cases where $i<3$ or $j<3$, should be treated separately; thus,

$$\begin{aligned}&b_{12}=2\sqrt{3},\quad b_{1j}=2[(-1)^{j-3}-1]\ \ (j\geq 3),\\&b_{21}=0,\quad b_{2j}=2\sqrt{3}[1+(-1)^{j-3}]\ \ (j\geq 3),\\&b_{i1}=b_{i2}=0\quad(i\geq 3);\end{aligned}\tag{C.4}$$

b_{ii} may also be determined as

$$b_{ii}=\int_0^1\phi_i\phi_i'\,\mathrm{d}\xi=\phi_i\phi_i|_0^1-\int_0^1\phi_i'\phi_i\,\mathrm{d}\xi,\tag{C.5}$$

from which one can simply conclude that $b_{ii}=0$, for all i.

Next and similar to b_{ij}, for c_{ij} $(i,j\geq 3)$ one can write

$$c_{ij}=\int_0^1\phi_i\phi_j''\,\mathrm{d}\xi=\frac{1}{\lambda_j^4}\int_0^1\phi_i\phi_j''''\,\mathrm{d}\xi,\tag{C.6}$$

in which the last integral, after successive integration by parts, becomes

$$c_{ij}=\frac{1}{\lambda_j^4}\left\{[\phi_i\phi_j'''-\phi_i'\phi_j''+\phi_i''\phi_j'-\phi_i'''\phi_j]_0^1+\int_0^1\phi_i''''\phi_j''\,\mathrm{d}\xi\right\}.\tag{C.7}$$

Eq. (C.7), after applying the boundary conditions and performing several manipulations, leads to

$$c_{ij}=\frac{4}{1-(\lambda_i/\lambda_j)^4}(\lambda_j\sigma_j-\lambda_i\sigma_i)\left[(-1)^{i+j-6}+1\right]\quad(i,j\geq 3),\tag{C.8}$$

in which $\sigma_i=[\cos(\lambda_i)-\cosh(\lambda_i)]/[\sin(\lambda_i)-\sinh(\lambda_i)]$[15]; also, $\phi_i'(0)=-2\lambda_i\sigma_i$ and $\phi_i'(1)=2(-1)^{i-3}\sigma_i\lambda_i$, and similarly for ϕ_j, have been utilized.

Similar to b_{ij}, c_{ij} should be found separately for cases where $i<3$ or $j<3$; thus,

$$\begin{aligned}&c_{12}=0,\quad c_{1j}=2\lambda_j\sigma_j[(-1)^{j-3}+1]\ \ (j\geq 3),\\&c_{21}=0,\quad c_{2j}=2\sqrt{3}[(-1)^{j-3}-1](\lambda_j\sigma_j-2)\ \ (j\geq 3),\\&c_{i1}=c_{i2}=0\quad(i\geq 3).\end{aligned}\tag{C.9}$$

Following a similar procedure to that in Appendix B of Païdoussis (1998), c_{ii} can be determined. One can easily find that $c_{11}=c_{22}=0$; however, for $i\geq 3$, c_{ii} becomes

$$c_{ii}=\lambda_i\sigma_i(2-\lambda_i\sigma_i)\quad(i\geq 3).\tag{C.10}$$

Appendix D. A discussion on the sharp jumps in the curves shown in Figs. 6 and 11

As seen in Figs. 6 and 11, for specific values of system parameters, u_{cr} experiences a sharp jump exactly where it is expected to reach a constant value. As discussed in detail in Section 4.3, this feature of the system may be linked to the *mode exchange* or *role reversal* phenomenon.

Determining where exactly these jumps start and end is a time-consuming task and needs a high level of accuracy in the numerical calculations. In other words, if, for example, the step by which the dimensionless flow velocity u_{cr} is varied in the analysis is reduced from $\Delta u=0.01$ to $\Delta u=0.001$, the jump associated with $\beta=0.2$ in Fig. 6 will emerge at $\kappa_0^*=10^{-7}$ instead of $\kappa_0^*=10^{-5}$, as shown in Fig. D1. Moreover, it is necessary to vary the system parameters, e.g. κ_0^*, in very small steps. However, it should be mentioned that the considerable effort necessary to determine the exact form of the jumps is mostly out of curiosity rather than for its practical importance. In fact, in practical applications and experiments, in many cases, parameters cannot be varied in such small steps; for example, for an elastomer pipe ($EI=7.63\times 10^{-3}$ N m^2) of

[15] See Kheiri et al. (2013a).

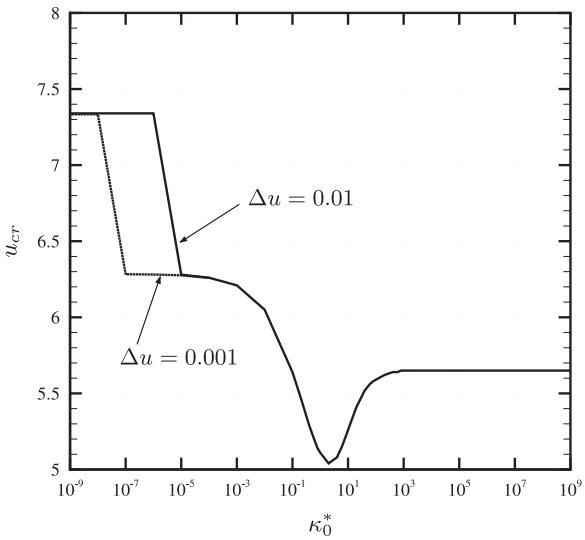

Fig. D1. Showing how the jump in the values of u_{cr} can be found at different values of κ_0^* if different levels of accuracy ($\Delta u = 0.01$ and $\Delta u = 0.001$) are used in the calculations.

length 0.401 m and external and internal diameters of, respectively, 0.0159 m and 0.00934 m, discharging water, $\Delta u = 0.01$ corresponds to $\Delta U \simeq 0.006$ m/s, which cannot be achieved in most apparatuses.

References

Ashley, H., Haviland, G., 1950. Bending vibrations of a pipe line containing flowing fluid. Journal of Applied Mechanics 17, 229–232.
Bajaj, A.K., Sethna, P.R., Lundgren, T.S., 1980. Hopf bifurcation phenomena in tubes carrying fluid. SIAM Journal of Applied Mathematics 39, 213–230.
Benjamin, T.B., 1961a. Dynamics of a system of articulated pipes conveying fluid. I. Theory. Proceedings of the Royal Society (London) A 261, 457–486.
Benjamin, T.B., 1961b. Dynamics of a system of articulated pipes conveying fluid. II. Experiments. Proceedings of the Royal Society (London) A 261, 487–499.
Bourrières, F.J., 1939. Sur un phénomène d'oscillation auto-entretenue en mécanique des fluides réels. Publications Scientifiques et Techniques du Ministère de l'Air, No. 147.
Casetta, L., Pesce, C.P., 2013. The generalized Hamilton's principle for a non-material volume. Acta Mechanica 224 (4), 919–924.
Chen, S.S., 1971. Flow-Induced Instability of an Elastic Tube. ASME Paper No. 71-Vibr-39.
Ch'ng, E., Dowell, E.H., 1979. A theoretical analysis of nonlinear effects on the flutter and divergence of a tube conveying fluid. In: Chen, S.S., Bernstein, M.D. (Eds.), Flow-Induced Vibrations, ASME, New York, pp. 65–81.
Daugherty, R.L., Franzini, J.B., 1965. Fluid Mechanics with Engineering Applications. McGraw-Hill, New York.
Edelstein, W.S., Chen, S.S., 1985. Flow-induced instability of an elastic tube with a variable support. Nuclear Engineering and Design 84, 1–11.
Feodos'ev, V.P., 1951. Vibrations and stability of a pipe when liquid flows through it. Inzhenernyi Sbornik 10, 169–170.
Firouz-Abadi, R.D., Askarian, A.R., Kheiri, M., 2013. Bending-torsional flutter of a cantilevered pipe conveying fluid with an inclined terminal nozzle. Journal of Sound and Vibration 332, 3002–3014.
Ghayesh, M.H., Amabili, M., Païdoussis, M.P., 2012. Thermo-mechanical phase-shift determination in Coriolis mass-flow meters with added masses. Journal of Fluids and Structures 34, 1–13.
Ghayesh, M.H., Païdoussis, M.P., 2010. Three-dimensional dynamics of a cantilevered pipe conveying fluid, additionally supported by an intermediate spring array. International Journal of Non-Linear Mechanics 45, 507–524.
Ghayesh, M.H., Païdoussis, M.P., Modarres-Sadeghi, Y., 2011. Three-dimensional dynamics of a fluid-conveying cantilevered pipe fitted with an additional spring-support and an end-mass. Journal of Sound and Vibration 330, 2869–2899.
Giacobbi, D.B., Rinaldi, S., Semler, C., Païdoussis, M.P., 2012. The dynamics of a cantilevered pipe aspirating fluid studied by experimental, numerical and analytical methods. Journal of Fluids and Structures 30, 73–96.
Giacobbi, D.B., Semler, C., Païdoussis, M.P., 2008. Numerical fluid–structure interaction study of a cantilevered pipe discharging or aspirating fluid via a computational fluid dynamics and finite element analysis model. In: Proceedings of the Sixth International Conference on Engineering Computational Technology. Paper 48, ETC2008, 2–5 September 2008, Athens, Greece.
Gregory, R.W., Païdoussis, M.P., 1966a. Unstable oscillation of tubular cantilevers conveying fluid. I. Theory. Proceedings of the Royal Society (London) A 293, 512–527.
Gregory, R.W., Païdoussis, M.P., 1966b. Unstable oscillation of tubular cantilevers conveying fluid. II. Experiments. Proceedings of the Royal Society (London) A 293, 528–542.
Guran, A., Plaut, R.H., 1994a. Stability of a fluid-conveying pipe with flow-dependent support stiffness. Journal of Applied Mechanics 61, 477–478.
Guran, A., Plaut, R.H., 1994b. Stability boundaries for fluid-conveying pipes with flexible support under axial load. Archive of Applied Mechanics 64, 417–422.
Hellum, A., Mukherjee, R., Bénard, A., Hull, A.J., 2013. Modeling and simulation of the dynamics of a submersible propelled by a fluttering fluid-conveying tail. Journal of Fluids and Structures 36, 83–110.
Housner, G.W., 1952. Bending vibrations of a pipe line containing flowing fluid. Journal of Applied Mechanics 19, 205–208.
Ibrahim, R.A., 2010. Overview of mechanics of pipes conveying fluids. Part I: fundamental studies. ASME Journal of Pressure Vessel Technology 132, 1–32.
Ibrahim, R.A., 2011. Mechanics of pipes conveying fluids. Part II: applications and fluidelastic problems. ASME Journal of Pressure Vessel Technology 133, 1–30.
Irschik, H., Holl, H.J., 2002. The equations of Lagrange written for a non-material volume. Acta Mechanica 153, 231–248.
Jendrzejczyk, J.A., Chen, S.S., 1985. Experiments on tubes conveying fluid. Thin-Walled Structures 3, 109–134.

Kheiri, M., Païdoussis, M.P., Amabili, M., 2013a. A nonlinear model for a towed flexible cylinder. Journal of Sound and Vibration 332, 1789–1806.
Kheiri, M., Païdoussis, M.P., Amabili, M., Epureanu, B.I., 2013b. Three-dimensional dynamics of long pipes towed underwater. Part 1: the equations of motion. Ocean Engineering 64, 153–160.
Kheiri, M., Païdoussis, M.P., Amabili, M., Epureanu, B.I., 2013c. Three-dimensional dynamics of long pipes towed underwater. Part 2: linear dynamics. Ocean Engineering 64, 161–173.
Kuiper, G.L., Metrikine, A.V., 2005. Dynamic stability of a submerged, free-hanging riser conveying fluid. Journal of Sound and Vibration 280, 1051–1065.
Kuiper, G.L., Metrikine, A.V., 2008. Experimental investigation of dynamic stability of a cantilever pipe aspirating fluid. Journal of Fluids and Structures 24, 541–558.
Kuiper, G.L., Metrikine, A.V., Efthymiou, M., 2007. Experimental investigation of the dynamic behaviour of a water intake riser. In: Proceedings of the 26th International Conference on Offshore Mechanics and Arctic Engineering, OMAE2007-29401, 10–15 June 2007, San Diego, USA.
Laithier, B.E., Païdoussis, M.P., 1981. The equations of motion of initially stressed Timoshenko tubular beams conveying fluid. Journal of Sound and Vibration 79, 175–195.
Li, W.L., 2000. Free vibrations of beams with general boundary conditions. Journal of Sound and Vibration 237, 709–725.
Lundgren, T.S., Sethna, P.R., Bajaj, A.K., 1979. Stability boundaries for flow induced motions of tubes with an inclined terminal nozzle. Journal of Sound and Vibration 64, 553–571.
McIver, D.B., 1973. Hamilton's principle for systems of changing mass. Journal of Engineering Mathematics 7, 249–261.
Meirovitch, L., 1967. Analytical Methods in Vibrations. The Macmillan Company, New York.
Mukhin, O.N., 1965. Stability of a Pipeline and Some Methods in Nonconservative Problems. Vestnik Moskovskovo Universiteta, Series I, Mathematics, 76–87.
Niordson, F.I., 1953. Vibrations of a Cylindrical Tube Containing Flowing Fluid. Kungliga Tekniska Hogskolans Handlingar, Stockholm, No. 73.
Noah, S.T., Hopkins, G.R., 1980. Dynamic stability of elastically supported pipes conveying pulsating fluid. Journal of Sound and Vibration 71, 103–116.
Païdoussis, M.P., 1970. Dynamics of tubular cantilevers conveying fluid. Journal of Mechanical Engineering Science 12, 85–103.
Païdoussis, M.P., 1998. Fluid–Structure Interactions: Slender Structures and Axial Flow, 1. Academic Press, London; Second Edition, 2014.
Païdoussis, M.P., 1999. Aspirating pipes do not flutter at infinitesimally small flow. Journal of Fluids and Structures 13, 419–425.
Païdoussis, M.P., Issid, N.T., 1974. Dynamic stability of pipes conveying fluid. Journal of Sound and Vibration 33, 267–294.
Païdoussis, M.P., Li, G.X., 1993. Pipes conveying fluid: a model dynamical problem. Journal of Fluids and Structures 7, 137–204.
Païdoussis, M.P., Luu, T.P., 1985. Dynamics of a pipe aspirating fluid, such as might be used in ocean mining. ASME Journal of Energy Resources Technology 107, 250–255.
Païdoussis, M.P., Semler, C., Wadham-Gagnon, M., 2005. A reappraisal of why aspirating pipes do not flutter at infinitesimal flow. Journal of Fluids and Structures 20, 147–156.
Païdoussis, M.P., 2010. The dynamics of cylindrical conduits containing flowing fluid. Computational Technology Reviews 1, 83–120.
Pramila, A., 1992. Undamped cantilever aspirating fluid may be stable. Rakenteiden Mekaniikka 25, 3–14.
Pramila, A., Laukkanen, J., Liukkonen, S., 1991. Dynamics and stability of short fluid-conveying Timoshenko element pipes. Journal of Sound and Vibration 144, 421–425.
Rao, S.S., 2007. Vibration of Continuous Systems. John Wiley & Sons, New York.
Ratigan, J.L., 2008. Brine String Integrity and Model Simulation. SMRI Technical Conference Paper, Galveston, TX, USA, pp. 273–293.
Rousselet, J., Herrmann, G., 1981. Dynamic behavior of continuous cantilevered pipes conveying fluid near critical velocities. Journal of Applied Mechanics 48, 943–947.
Semler, C., Li, G.X., Païdoussis, M.P., 1994. The non-linear equations of motion of pipes conveying fluid. Journal of Sound and Vibration 169, 577–599.
Stangl, M., Gerstmayer, J., Irschik, H., 2008. An alternative approach for the analysis of nonlinear vibrations of pipes conveying fluid. Journal of Sound and Vibration 310, 493–511.
Sugiyama, Y., Kawagoe, H., 1975. Vibration and stability of elastic columns under the combined action of uniformly distributed vertical and tangential forces. Journal of Sound and Vibration 38, 341–355.
Sugiyama, Y., Tanaka, Y., Kishi, T., Kawagoe, H., 1985. Effect of a spring support on the stability of pipes conveying fluid. Journal of Sound and Vibration 100, 257–270.
Verichev, S., Metrikine, A., Plat, R., Hendrikse, H., 2011. Dynamics of the vertical hydraulic transport system for deep sea mining. In: Proceedings of the ASME 2011 30th International Conference on Ocean, Offshore and Arctic Engineering, OMAE2011-49464, 19–24 June 2011, Rotterdam, The Netherlands.
White, F.M., 2008. Fluid Mechanics, Sixth edition McGraw-Hill, New York.
Xia, J.X., Ni, J.R., Mendoza, C., 2004. Hydraulic lifting of manganese nodules through a riser. ASME Journal of Offshore Mechanics and Arctic Engineering 126, 72–77.
Ziegler, H., 1968. Principles of Structural Stability. Blaisdell, Waltham, Mass.